
SCHOOL OF ADVANCED STUDIES
Doctorate course in
BIOLOGY
PhD thesis

# Interaction between GroES and Proteasomes: structural and functional characterization

Cycle XIX

Scientific-sector BIO/10

PhD candidate
***Dr. Francesca Montecchia***

Tutor
***Prof. Mauro Angeletti***
***Dr. Anna Maria Eleuteri***

2003/04 – 2005/06

# SUMMARY

# INTRODUCTION

Interactome is the whole set of molecular interactions in cells. When referred to in terms of proteomics, it concerns protein-protein interaction.

These activities are very important to fully understand properties and operations of cellular systems. Recently, together with the application of experimental techniques for the determination of protein interaction networks and protein complexes, a number of computational methods based on sequence and genomic information have emerged. Among these, orthology-based methods assume that two proteins may interact if each one has at least an ancestor in its phylogenetic tree interacting with at least an ancestor of the other.

The purpose of this work was the evaluation of the interaction between two potential binding partners, namely bovine MPC and GroES, and presented to main phases: a preliminary *in silico* study, aimed to the assessment of feasibility of the interaction, and an *in vitro* study, based on fluorimetric, chromatographic and SPR approaches, directed to the confirmation and characterization of the interaction.

## *IN SILICO STUDY*

### *Orthology-Based Method For Proteins Interaction Prediction*

In order to build a model for the prediction of possible interaction between proteins, we designed a workflow, using the amino acidic sequences of a two proteins (namely A and B) as input. In the first step we searched for A and B orthologues separately, using the Cluster of Orthologous (COG) database (http://www.ncbi.nlm.nih.gov/COG/new), which contains a classification of proteins, from seven complete genomes and five major phylogenetic lineages, according to their orthologous relationships. Orthologous proteins are a class of proteins sharing a common ancestor, successively separated by a speciation event. Normally, but not necessarily, they share the same function. We obtained two sets of A and B orthologues (AO and BO, respectively). Then we searched for a subset *I* of the Cartesian product *AOxBO* set, containing all couples of proteins which are known to interact. In our approach, we used the *Biomolecular Interaction Network Database* (BIND)[1] (http://bond.unleashedinformatics.com/), the *Biomolecular Relations in Information Transmission and Expression* (BRITE)[2] (http://www.genome.jp/kegg/brite.html ) and the Database of Interacting Proteins (DIP)[3] (http://dip.doembi.ucla.edu/ ) as interaction datasets. If *I* was not null, we could conclude that A and B proteins should interact. Figure 1 shows the workflow of all the activities for protein interaction prediction using orthology-based method.

### *Cluster Orthologous Group (COG) DATABASE*

The availability of multiple, essentially complete genome sequences of prokaryotes and eukaryotes enhanced both the demand and the opportunity for the construction of an evolutionary classification of genes from these genomes. Such a classification system based on orthologous relationships between genes appears to be a natural framework for comparative genomics and should facilitate both functional annotation of genomes and large-scale evolutionary studies. The Clusters of Orthologous Groups of proteins (COGs)[4] contains a classification of proteins, from seven complete genomes and five major phylogenetic lineages, according to their orthologous relationships. KOGs added in 2003[5] are the clusters of predicted orthologs for 7 eukaryotic genomes. The COG collection currently consists of 138,458 proteins, which form 4873 COGs and comprise 75% of the 185,505 (predicted) proteins encoded in 66 genomes of unicellular organisms. The eukaryotic orthologous groups (KOGs) include proteins from 7 eukaryotic genomes: three animals (the nematode *Caenorhabditis elegans*, the fruit fly *Drosophila melanogaster* and *Homo sapiens*), one plant, Arabidopsis thaliana, two fungi

(*Saccharomyces cerevisiae* and *Schizosaccharomyces pombe*), and the intracellular microsporidian parasite *Encephalitozoon cuniculi*. The current KOG set consists of 4852 clusters of orthologs, which include 59,838 proteins, or approximately 54% of the analyzed eukaryotic 110,655 gene products. Compared to the coverage of the prokaryotic genomes with COGs, a considerably smaller fraction of eukaryotic genes could be included into the KOGs; addition of new eukaryotic genomes is expected to result in substantial increase in the coverage of eukaryotic genomes with KOGs. Examination of the phyletic patterns of KOGs reveals a conserved core represented in all analyzed species and consisting of approximately 20% of the KOG set. This conserved portion of the KOG set is much greater than the ubiquitous portion of the COG set (approximately 1% of the COGs). In part, this difference is probably due to the small number of included eukaryotic genomes, but it could also reflect the relative compactness of eukaryotes as a clade (*a taxonomic group of organisms classified together on the basis of homologous features traced to a common ancestor*) and the greater evolutionary stability of eukaryotic genomes.

***Protein Interaction DATABASES***

Protein interaction data are mainly derived from genome wide, high-throughput yeast two-hybrid experiments, in which interactions are measured between all genes pairs in a genome. More than 4000 unique protein interactions were observed between yeast proteins in three large-scale experiments[6-8]. More recently, complexes of yeast proteins have been isolated, and the protein constituents have been identified by mass spectrometric approaches[9-11], thereby identifying hundreds of additional interactions among yeast proteins. A test similar to the high-throughput yeast two-hybrid experiments, performed on bacterial proteins, identified more than 1200 interactions between proteins of the human gastric pathogen H. pylori[11]. In addition to large-scale experimental approaches, a number of groups have been attempting to cull the previously measured protein-protein interactions from biological literature[12,13]. This systematic collection of protein interaction data provides necessary checks on the quality of the large-scale interaction data. Large-scale protein interaction data have varied widely in accuracy[14], but many interactions in the databases have been observed by multiple experimental methods, providing some measure of confidence in the correctness of these interactions. In our *in silico* experiment we have considered three protein-protein interactions databases: BIND, BRITE and DIP.

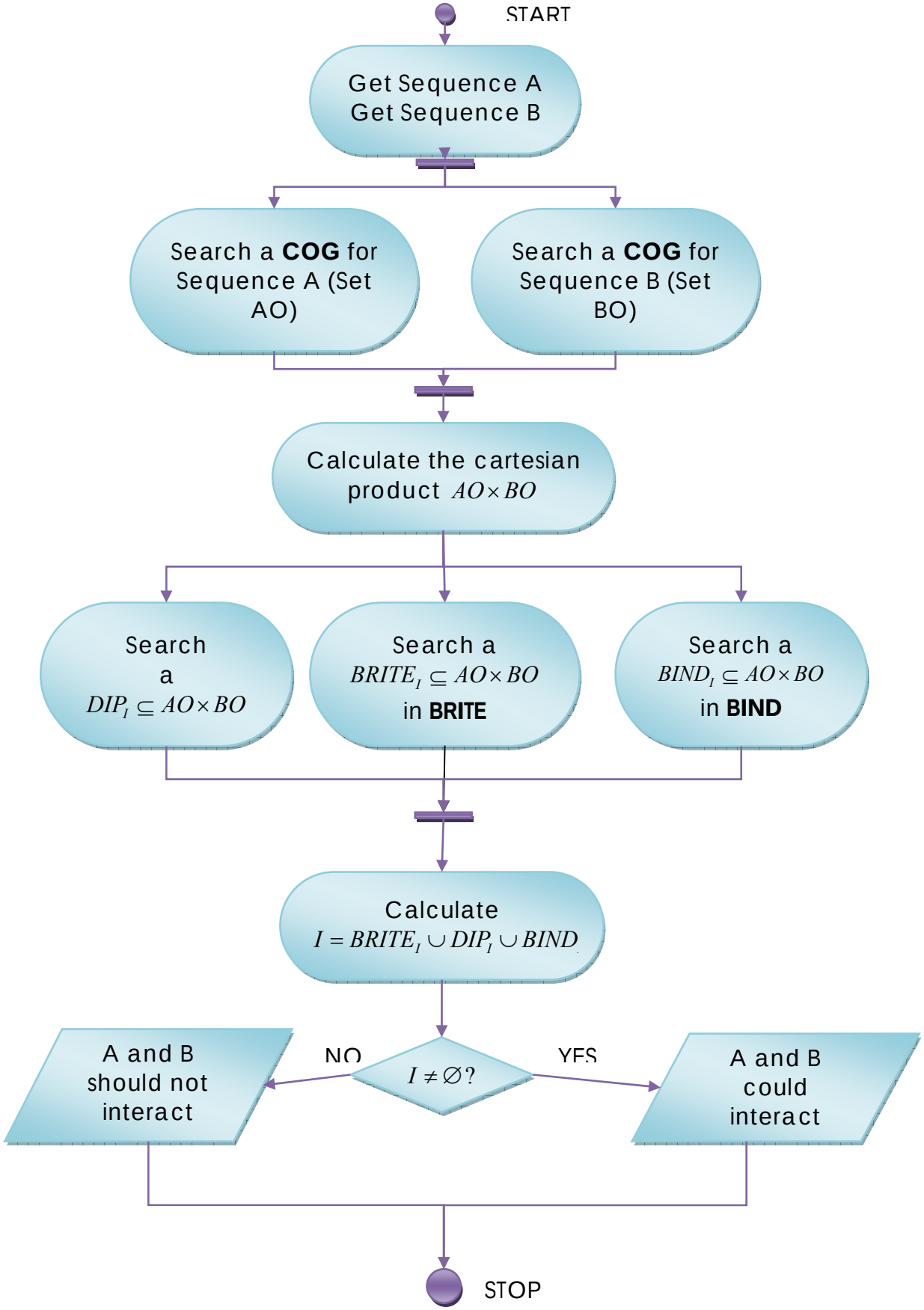


**Fig.1.** Workflow of an orthology-based method for proteins interaction prediction

BIND and DIP database combine the interactions from the large-scale screens with the interactions extracted from the literature. As of this writing, DIP (http://dip.doe-mbi.ucla.edu) currently contains 55894 interactions between 19206 proteins, from several organisms (*Drosophila melanogaster*, *Saccharomyces cerevisiae*, *Escherichia coli*, *Caenorhabditis elegans*, *Homo sapiens*, *Helicobacter pylori*, *Mus musculus*, *Rattus norvegicus*). BIND (http://bond.unleashedinformatics.com/) currently contained approximately more than 100 000 interactions. Approximately 71% of BIND records arise from high-throughput experiments. There are 58 266 protein–protein interactions and 4225 genetic interactions in BIND. There are also 874 protein–small-molecule interactions in BIND, but it should be noted that we have not yet undertaken any deliberate metabolic pathway annotation, and that small molecules from the Protein Data Bank (PDB) are not counted in this number. A total of 19 348 BIND biopolymer–biopolymer interaction records are derived from the PDB structures with full annotation of atomic contacts, after discarding crystal symmetry artefacts and grouping redundant structure interfaces (fig. 2). Almost half of these data represents biological oligomer interactions. Another 25 857 BIND records are protein–DNA interactions, with 23 865 of these originating from high-throughput chromatin-immunoprecipitation-style transcription-factor binding experiments, representing a very fast growing experimental trend. In total, 31 972 protein sequences, as well as 4560 DNA sequences and 759 RNA sequences are represented in BIND, and all of these records reflect the content of 11 649 unique publications. Organisms represented in BIND include *Saccharomyces cerevisiae* (48 151 records), *Drosophila melanogaster* (21 309), Homo sapiens (13 902), *Caenorhabditis elegans* (5266), *Mus musculus* (3823), *Helicobacter pylori* (1470), *Bos taurus* (1064), human immunodeficiency virus 1 (442), *Gallus gallus* (318) and *Arabidopsis thaliana* (180) with over 10000. BIND records arising from other taxonomies. A total of 901 taxa are represented in BIND. The Database of Interacting Proteins (DIP: http://dip.doe-mbi.ucla.edu) is a database that documents experimentally determined protein–protein interactions. It provides the scientific community with an integrated set of tools for browsing and extracting information about protein interaction networks. As of September 2001, the DIP catalogues ~11 000 unique interactions among 5900 proteins from >80 organisms; the vast majority from yeast, *Helicobacter pylori* and human. Tools have been developed that allow users to analyze, visualize and integrate their own experimental data with the information about protein–protein interactions available in the DIP database. Biomolecular Relations in Information Transmission and Expression (BRITE; http://www.genome.ad.jp/brite/) is a database of binary relations for computation and comparison of graphs involving genes and proteins. It is not a fully developed database yet, but its purpose in KEGG is to expand the collection of the generalized

protein interactions that underlie the KEGG pathway diagrams, especially direct protein–protein interactions obtained by systematic experiments such as yeast two-hybrid systems, and gene expression relations of transcription factors and transcribed gene products. BRITE will integrate the generalized protein interactions with other diverse sets of binary relations, including sequence similarity relations stored in the SSDB database, expression similarity relations obtained by cluster analysis of the EXPRESSION data, positional correlations in the GENES genome maps and cross-reference links between database entries in the LinkDB database, towards automating logical reasoning steps to understand functions.

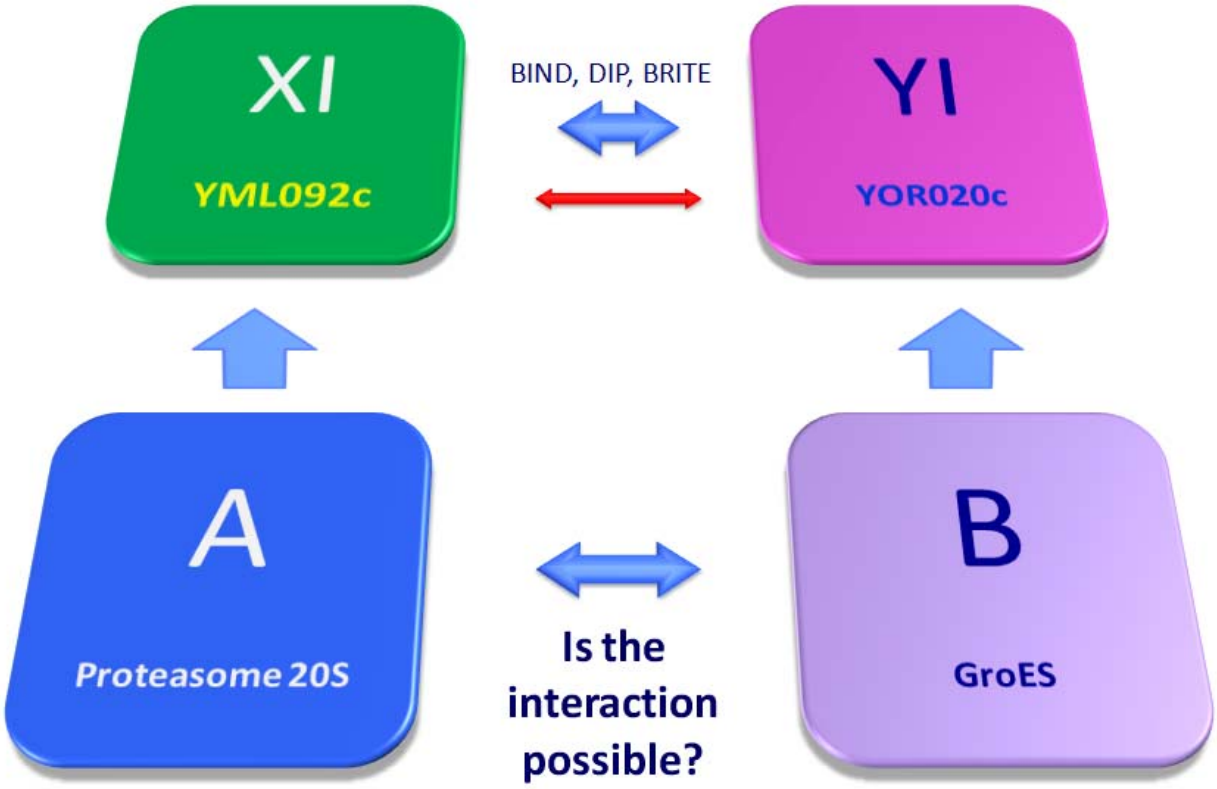


**Fig. 2:** Schematic representation of proteins interaction prediction.

## *Structure and function of the GroE chaperone*

Historically, GroE proteins from *Escherichia coli* were the first chaperone proteins to be studied on a molecular level[15,16]. Chaperonins are a diverse class of proteins, whose functions include roles in protein trafficking, protein assembly, and proteins folding[17].

The chaperonin system of *Escherichia* coli comprises two proteins, b-cpn60 (GroEL) and b-cpn10 (GroES)[18]. These chaperonins can modulate the refolding of protein under

"nonpermissive" conditions - i.e., conditions that do not allow spontaneous folding. Examples of proteins that undergo chaperone-dependent refolding include ribulose-1,5-bisphosphate carboxylase (Rubisco), citrate synthase, and rhodanese. In these cases the refolding reaction requires both chaperonin proteins as well as MgATP and $K^+$ [19]. Homologous chaperonin systems have been detected in mammalian mitochondria[20] and in chloroplast[21]. *E.coli* proteins are encoded by separate genes contained in the same *groE* operon, with GroES positioned first[18]. Of the two proteins, GroEL has been the most extensively studied. GroEL molecule is a complex assembly comprising 14 identical 57-kDa subunits. The transitions between the different functional states of the chaperone are triggered by a set of domain movements which in turn are controlled by the binding of ATP and the co-chaperone GroES.

The first images of the GroE chaperone were obtained by electron microscopy [22,23]. They showed cylindrical particles containing a central channel, which could be occupied by a polypeptide substrate[24-26]. A more detailed picture became available with the X-ray structure of GroEL[27]. It confirmed that the GroEL molecule resembles a barrel with dimensions of 137 Å (diameter) and 146 Å (height). Its 14 subunits are arranged in two rings stacked back to back. The two rings enclose two separate cavities (45 Å wide) that serve as folding compartments for polypeptide substrates. Each GroEL subunit can be dissected into three distinct domains[27]. The equatorial domains (residues 6–133 and 409–523) constitute the central part of the cylinder and consist mainly of α-helices. They serve as the foundations of the GroEL oligomer, since they mediate all inter-ring contacts, and most of the intra-ring contacts. They also contain the binding pockets for ATP, which are facing toward the inside of the central cavity.

In contrast to the equatorial domain, the apical domain (residues 191–376) is considerably less ordered. It is located at the opening of the GroEL cylinder (Fig. 3) and contains the binding site for both GroES and the polypeptide substrate. Polypeptide binding occurs in a hydrophobic groove, which is formed by two helices facing the central channel[28,29]. This is in agreement with results of an earlier analysis employing site-directed mutagenesis[30]. The bound substrate is stabilized mainly by hydrophobic interactions, but hydrogen bonds between its peptide backbone and the surrounding polar surface of the apical domain may contribute as well. Importantly, this hydrophobic groove is also responsible for the binding of GroES [31].

The intermediate domain (residues 134–190 and 377– 408) serves as a molecular hinge connecting the apical domain with the equatorial domain. Accordingly, its main function is the transmission of allosteric signals between both domains, thus establishing a tight coupling between nucleotide binding and GroES/polypeptide binding.

***The interaction between GroES and GroEL***

The co-chaperone, GroES (fig. 3 A), is a dome-shaped heptamer with diameter of 75 Å and a height of 30 Å[32]. It consists almost exclusively of β-sheets. Residues 16–33 form the so-called mobile loops, flexible extensions that dangle from the GroES molecule like the tentacles of a jellyfish[33,34]. Binding of GroES occurs at the apical domains of the GroEL tetradecamer (fig. 3 B) and requires that the nucleotide binding sites of the respective GroEL ring are occupied by either ATP or ADP[23,35,36]. Upon association, the mobile loops of GroES bind to the hydrophobic peptide binding groove of GroEL and become immobilized[31,33]. Because of the common seven-fold symmetry of both proteins, binding is thought to be highly cooperative. Upon binding of its co-chaperone, the GroEL molecule undergoes major structural rearrangements that are pivotal to its functional cycle (fig. 3 B, C)[31,37]. First, the apical domains of the *cis* ring, i.e. the ring target of binding with GroES, swing upward by ~60° and rotate outward by ~90°. As a result, the diameter of the central cavity almost doubles, and its volume increases from 85,000 $Å^3$ to 175,000 $Å^3$. Second, the hydrophobic residues, which form the peptide binding site of GroEL, are moved away from the cavity surface and become buried within the wall (fig. 3 C). Thus, the surface of the *cis* cavity becomes largely hydrophilic. Third, GroES now blocks the exit of the cavity. As a result, the *cis* cavity is converted from an acceptor site for hydrophobic polypeptides into a closed microenvironment for protein folding. Depending on the experimental conditions, two types of complexes between GroES and GroEL have been detected by electron microscopy. In the presence of ADP or micromolar concentrations of ATP, GroES binds to only one end of the GroEL cylinder forming asymmetric 'bullets' (see fig. 3 B)[23,26]. At ATP concentrations in the millimolar range, symmetrical 'footballs' have been observed in which both ends of the GroEL particle are capped with GroES[38-40]. It is assumed that the 'ADP bullet', i.e. the $GroES_7{\cdot}ADP_7{\cdot}GroEL_7/GroEL_7$ complex, represents the 'acceptor state' of GroE[41] , which captures an unfolded polypeptide. The footballs presumably reflect a transient species that is formed during the functional cycle .

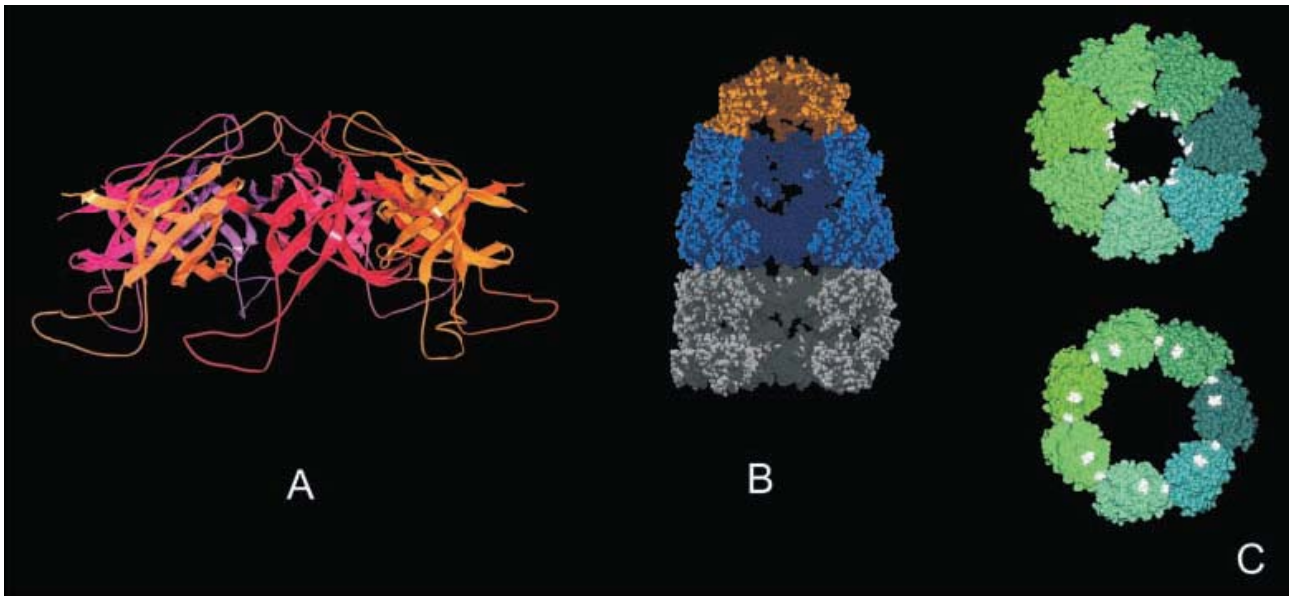


**Fig. 3:** Structure of the GroE chaperone from *E. coli*[31,32]. (*A*) Side view of the GroES heptamer. The individual subunits (in shades of red) consist mainly of *b* sheets and form a dome with a diameter of 75 Å. The flexible extensions on the bottom are the so-called mobile loops that mediate binding to GroEL. (*B*) Cross-section of a GroE 'bullet'. Each GroEL ring encloses a cavity that serves as a folding compartment for a polypeptide substrate. Some residues of the equatorial domains have not been resolved in the crystal structure, giving the wrong impression that the two cavities are contiguous. Binding of GroES (orange) to the top GroEL ring (blue) blocks the access to the upper cavity and concomitantly induces an en bloc movement of the apical domains. (*C*) Changes in the GroEL structure upon binding of GroES. In this top view, the seven subunits comprising one ring of GroEL are shown in shades of green and blue. The equatorial domains have been omitted for sake of clarity. The hydrophobic residues in the apical domains important for binding of polypeptide and GroES are shown in white. In the absence of GroES (top panel), these residues coat the inside of the central cavity and account for the high affinity for unfolded polypeptides of this state. Upon binding of GroES (lower panel) the apical domains rotate outwards by ~ 90°. The hydrophobic patches become buried in the subunit interfaces, rendering the inner surface of the cavity mainly hydrophilic and causing the release of a bound polypeptide. Concomitantly, the diameter of the cavity increases from 45 to 80 Å.

### *Allosteric interactions within the GroE chaperone*

Although each GroEL ring consists of seven subunits, it represents a single operational unit[42,43]. This behaviour is the consequence of a framework of allosteric interactions that coordinates the binding properties of the single subunits. There are two levels of cooperativity within the GroEL molecule. First, subunits of the same ring are subject to positive cooperativity. As an example, binding of ATP to one GroEL subunit promotes the binding of ATP to the other six subunits of the same ring[36,44,45]. Second, there is a negative cooperativity between the rings, i.e. the binding of ATP to one ring reduces the affinity for ATP of the second ring[44,46]. These homotropic effects can be described by a model of nested cooperativity[47] (fig. 4).

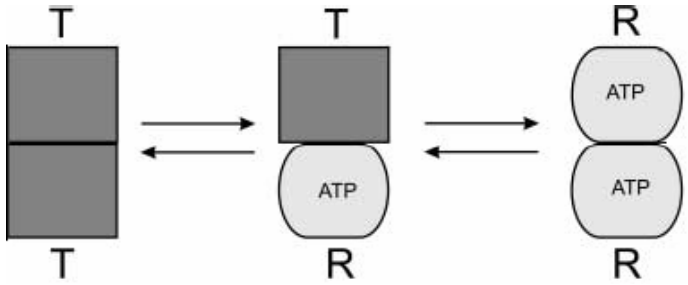


**Fig. 4:** Model of nested cooperativity in GroEL[48]. Each rectangle (square or round) represents a single ring. Owing to the positive intraring cooperativity, all seven subunits within one ring adopt the same state. In the absence of ligands, GroEL is predominantly in the TT state (left). In the presence of low concentrations of ATP, the equilibrium is shifted towards the TR state (middle), because ATP preferentially binds to the R conformation. At higher concentrations of ATP, transition to the RR state occurs.

Each GroEL subunit can adopt one of two states: the (relaxed) R state, and the (tense) T state, which differ in their affinity for nucleotide and protein ligands[48]. The R state is characterized by a high affinity for ATP and a low affinity for polypeptides, whereas the T state has a low affinity for ATP and a high affinity for polypeptides. Owing to the positive intra-ring cooperativity, each ring is either in the R form or in the T form. Thus, the GroEL tetradecamer can adopt the configurations TT, TR, and RR (fig. 4). In the absence of nucleotides, GroEL is preferentially in the TT state. Low concentrations of ATP shift the equilibrium to the RT state, in which the R ring is completely occupied with nucleotide, whereas the T ring is empty. Because of the negative interring cooperativity, the transition to the RR state only occurs at higher ATP concentrations (>100 μM). The cochaperone GroES, on the other hand, seems to reduce the negative interring cooperativity, since its binding to the RT state promotes the transition to the RR state[48]. This is consistent with the finding that in the 'ATP bullet' complex ($GroES_7 \cdot ATP_7$ $GroEL_7/GroEL_7$) the *trans* ring shows a decreased affinity for polypeptides[49].

### *The functional cycle of the GroE chaperone*

GroE-mediated folding requires the polypeptide substrate to participate in a cycle which can be dissected into three steps: capture, sequestration/folding and release[50]. The cycle starts when a polypeptide is captured by GroE (fig. 5, step 1). As mentioned above, a potential substrate is recognized by virtue of its exposed hydrophobic surfaces. The acceptor state of GroE likely is the 'ADP bullet', in which the *trans* ring (i.e. the ring opposite of GroES) is in the high-affinity T form.

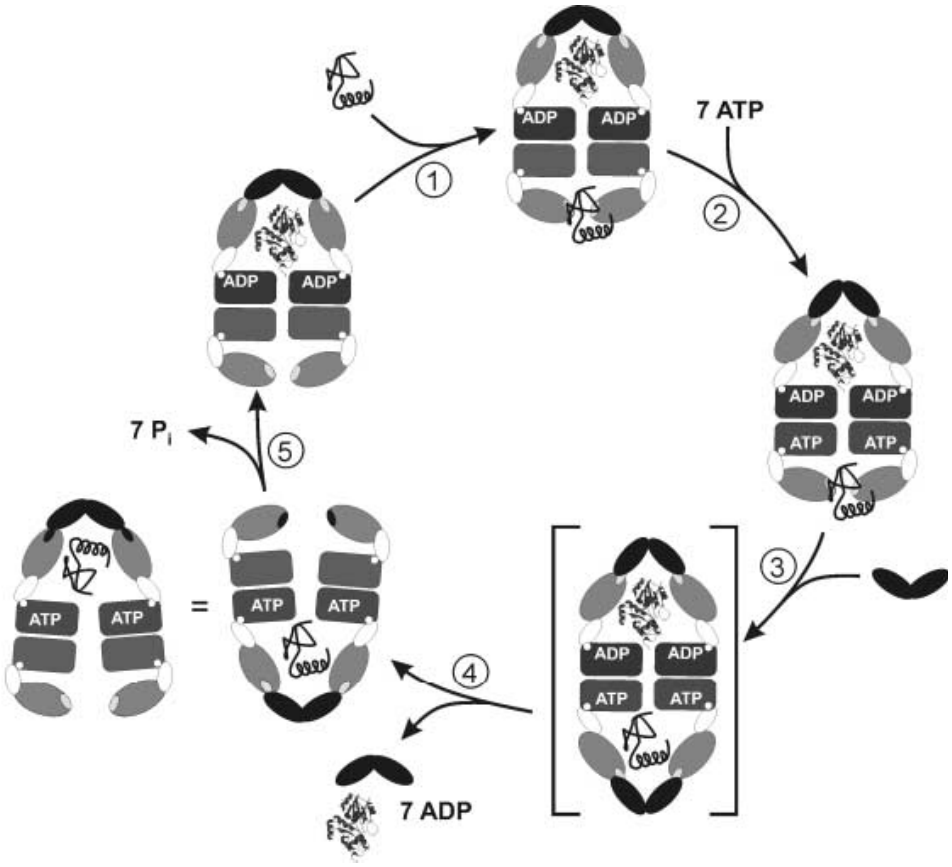


**Fig. 5:** Model of the functional cycle of the GroE chaperone. Although GroEL is composed of two rings, the functional cycle is best described on the level of single rings, which represent the operational units of the chaperone. While both rings are active at the same time, they are in different phases of the cycle. Processing of an individual substrate polypeptide requires two revolutions of the GroE cycle during which the polypeptide remains associated with the same GroEL ring. For graphical reasons, the orientation of the GroE complex is reversed after step 4. The cycle of GroE-assisted folding can be dissected into three steps: capture, encapsulation/folding and release. During capture (1), a hydrophobic polypeptide is prevented from aggregation by binding to GroEL. The acceptor ring (bottom ring) is nucleotide free and therefore has a high affinity for the polypeptide. Binding of ATP (2) and GroES (3) to this ring induces a set of structural changes in GroEL. Most important, the affinity for the bound polypeptide is decreased, and it is released into the closed cavity where folding begins. Subsequent hydrolysis of ATP (5) induces a second conformational change in GroEL (top ring), which allows the bottom ring to bind polypeptide and initiate a new cycle. Upon binding of ATP and GroES in the next round, GroES is displaced from the top ring, and the substrate polypeptide is released (4). The formation of the symmetric complex shown in brackets is controversial.

Consequent binding of ATP and GroES to this ring (fig. 5, steps 2 and 3) triggers a series of conformational changes in the GroEL molecule. As a result,

1) The affinity for both ADP and GroES in the *trans* ring decreases, causing the dissociation of both ligands (fig. 5, step 4)[51-53].
2) GroES covers the opening of the new *cis* cavity, thereby creating a closed compartment which sequesters the polypeptide substrate[41,54].
3) The polypeptide binding site in the *cis* ring becomes buried within the cavity wall, causing the discharge of the polypeptide into the *cis* cavity.
4) The size of the cavity increases, giving the polypeptide sufficient room to undergo the structural rearrangements required for productive folding[31].

The cycling ends when the polypeptide molecule has reached a conformation that is no longer recognized by GroEL. For some monomeric proteins like rhodanese, this exit point may be the native state[41,54]. In general, however, it will be a committed state in which the protein has not yet reached its native conformation, but no longer requires the assistance of GroE[55,56].

Hydrolysis of the bound ATP (fig. 5, step 5), which takes ~10 s at 25 °C[44], represents the rate-limiting step in the cycle and thus serves as a timer for encapsulation[49].

Once the ATP is hydrolyzed, the chaperone has completed its cycle and the next round starts, in which now the opposite ring will be charged with a polypeptide substrate. The release of the encapsulated protein occurs upon the subsequent binding of GroES/ATP (fig. 5, step 4).

At this stage, the ejected polypeptide is thought to undergo kinetic partitioning[53,57]. Molecules unrecognized by GroEL (native, committed or dead-end, see above) do not participate any longer in cycling. The remaining molecules may rebind and undergo another round of the GroE cycle, or bind to other molecular chaperones, or fold/assemble in bulk solution. The relative fractions of these species likely depend on the nature of the polypeptide as well as on the cellular context.

It is reasonable to assume that GroEL can process two substrates at a time, as shown in figure 5. According to this model, both rings (operational units) are active, although they are in different phases of the chaperone cycle[49,58]. As an example, the top ring after step 3 is loaded with a polypeptide that already has undergone folding in the cavity, and will become ejected in the next step. The polypeptide bound to the bottom ring, on the other hand, will be released into the cavity where folding is initiated. Thus, binding of GroES in step 3 has a dual function: it sequesters a 'new' polypeptide in the *cis* cavity, and it releases GroES and the processed polypeptide from the *trans* ring. In an alternative model, only one GroEL ring at a time is loaded with a polypeptide, whereas the second ring passes through the cycle in an empty state. Owing to the limited volume of the cavity, GroE-mediated folding as shown in figure 5 is restricted to polypeptides smaller than ~ 60 kDa[59,60]. Although larger proteins can bind to GroEL, they cannot become encapsulated underneath GroES.

## *The complex of the multicatalytic protease*

### *The control of the protease through protein autocompartimentation*

Protein degradation is fundamental in the regulation of several physiological process like the maintaining of homeostasis during continuous reconstruction of cellular structures, both during the development and as response to externals stimulations, the removal of misfolded proteins after mutations, oxidative stress or heat, the elimination of regulatory proteins in defined moments (cycline, transcriptional factors, components of signal transduction paths and the degradation of external antigens and the consequent production of immunocompetent peptides). Since the degradation represents a possible risk, it has to be carefully controlled to prevent the removal of proteins not destined to proteolysis. A potential mechanism of control of the protein degradation is represented by compartmentalization, defined as the ability to define the proteolytic action to sites that result accessible only to protein with degradation signals. The prokaryotic cells that do not posses membrane compartments or vescicular transport systems have developed a different compartmentalization, defined as autocompartimentalization, defined as the formation of a commune architecture where different proteolytic subunits are able to form cylindrical structures where the catalytic sites are confined in the internal cavities (several nanometres of diameter) [61].

The access to the internal compartments is generally limited to unfolded polypeptides, able to pass through narrows pores or entering channels. The target proteins must be able to interact with a system able to bind to them and to be presented to the catalytic site in an unfolded way.

Since protein unfolding and folding are related mechanism, it is supposed that the unfolding complexes are ATPasic ones, partially similar to chaperonine and defined as inverted chaperonine or unfoldase. Since their action request the hydrolysis of ATP, the protein degradation is an energy-demanding process. The proteasic autocompartimentalization is common for all life domains: archobacetria, eubacteria ad eukaryotes. This is a testimony of the importance of one of the evolution principles. Differing from organelles, the autocompartimentalization offers more flexibility: by having appropriate localization signals, such proteasic complexes can reach different cellular districts where is necessary their action.

### *The proteolitic system ubiquitin-proteasome*

The turnover in normal and altered proteins is performed principally by a proteolitic system ATP-ubiquitin-dependent, present in nucleus and cytoplasm of eukaryotic cells but also in

eubacteria and in archobacetria [61-63]. The protein substrates destined to degradation are marked through covalent binding with a number of molecules of a small protein, namely ubiquitin.
This protein is constituted by 76 amino acids with a molecular weight of 8,5 kDa, and it is highly conserved through evolution. The poli-ubiquitinization happens through the sequential action of three enzymes (fig. 6): an ATP-dependent enzyme ubiquitin dependent (E1), an ubiquitin conjugating enzyme (E2) and ubiquitin ligase (E3).

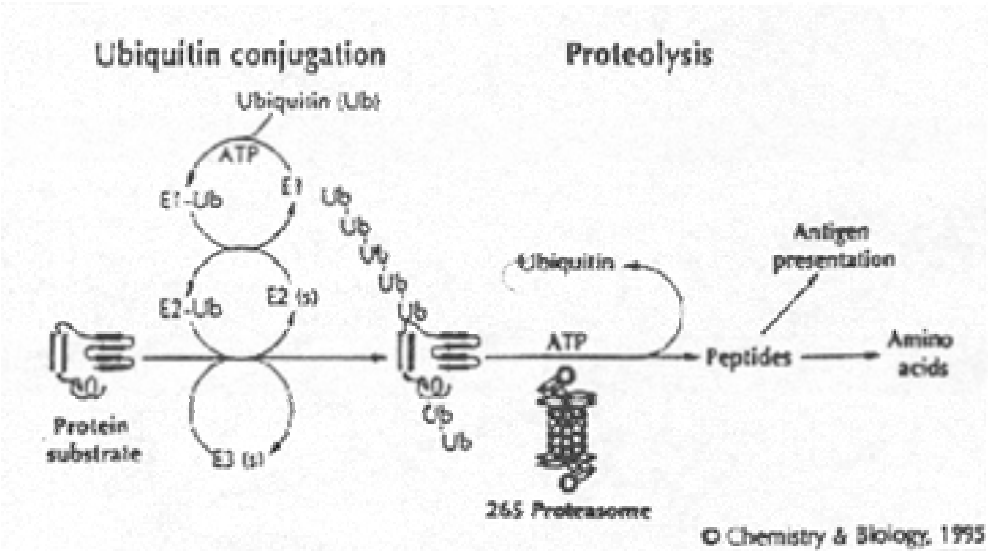


**Fig. 6:** Schematic representation of the polyubiquitinizzation of a proteic substrate and further recognize and degradation by a part of the multicatalitic protease complex

The three enzymes are able to act simultaneously through a covalent attack with the C-terminal of ubiquitin to the amino group of a lysine residue of the target protein. Other ubiquitin molecules are able to link to the first by forming a long linear or ramified chain. The polyubiquitinated chains are first recognized and degraded by a subunit of an ATP-dependent proteolytic complex, the proteasome 26S. This latter is a 2000 kDa protease consisting of a catalytic core, the proteasome 20S, with a molecular weight of 700 kDa. The proteasome 20S shows a multiproteic structure with a cylindrical structure containing several peptidasic activities, namely MPC or Multicatalytic Protease Complex.

***The proteasome 20S - Structure***

The proteasome from the *Archobacteria Thermoplasma Acidophilum* is the prototype for the quaternary structure and the enzyme topology. Its 28 substructures represent two homologues genetic products ($\alpha$ e $\beta$), each present in 14 copies for each proteasolmal molecule [61,64,65]. The

subunits are arranged to form four heptameric rings with the α subunits forming the two external rings and the subunits β forming the internal rings. Collectively, they form a cylindrically-shaped complex, about 15 nm long, and with a diameter of 11 nm, including the three internal cavities of 5nm of diameter delimitated by four close constrictions. The central cavity is formed by two adjacent β rings, while the two external cavities are delimited by a β and α ring. In eukaryotes, the subunits represent 14 genetic products; seven of them are homologues of the subunit α of the *Thermoplasma* and the other seven homologues of the β subunits.

The relative positions of α and β subunits of eukaryotes are analogous to those of the proteasome from the *Thermoplasma*, each ring containing a complete set of the seven genetic products. Thus the proteasome is a multimeric dimer with a symmetric axis passing through the two α and β rings, whose subunits point their active sites toward the inner surface of the central channel. The ternary structure of α non-catalytic and β catalytic subunits is very similar: each one is constituted by a sandwich of five antiparallel β sheets in contact with α helices.

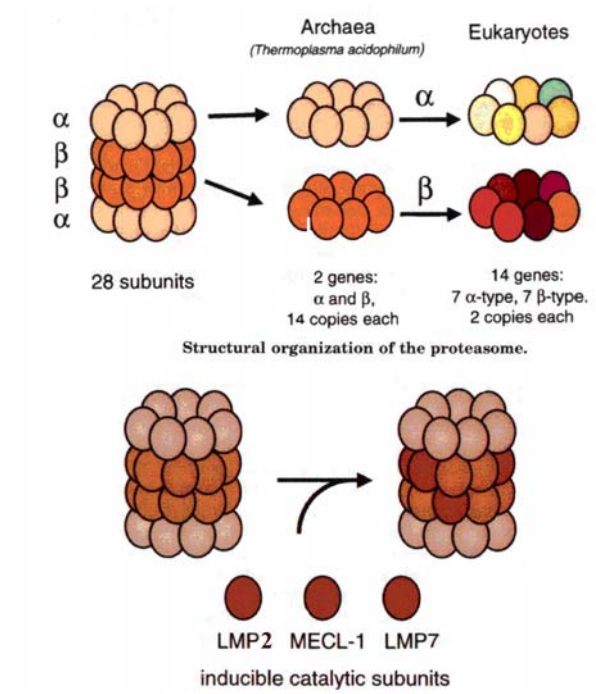


**Fig. 7:** Structural organization of the proteasome 20S (upper) and schematic representation of the subunit substitution in the immunoproteasome (below)

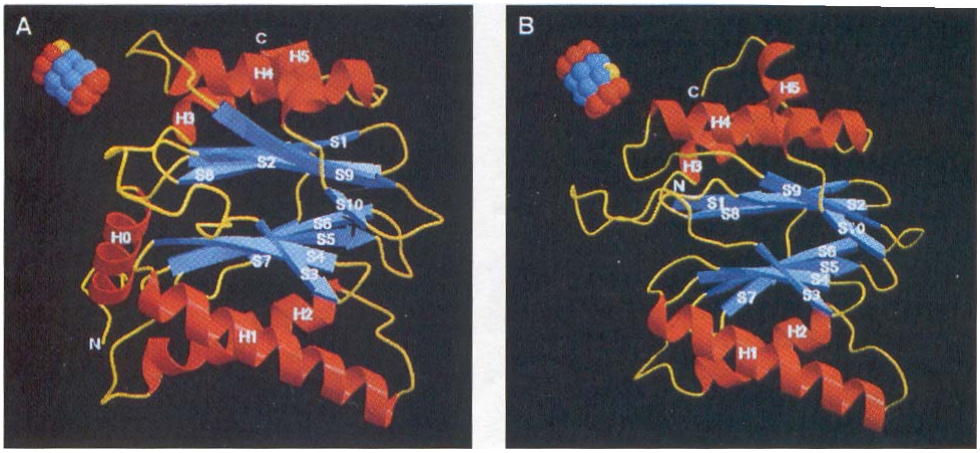


**Fig. 8:** Ribbons representation of the α subunits (A); the α helix are indicated with H, the β sheets with S. The helix HO at the NH2-terminal extremity represents the internal side of the proteosomal complex. In the barrel structure in the upper left, orientated in the same way, is indicated with a yellow sphere; (B) represents the β subunit.

The H1 and H2 helices modulate the interaction between α and β rings (β-trans-α); H3 and H4 helices, on the other hand, are the main links between the two β rings (β-transβ). The major difference between α and β subunits is the presence of a N-terminal extension on the α subunit (α-helix-HO) that crosses the central sandwich. The N-terminal extension can be found in the upper part of the α-ring, close to the access of the pre-cavity, likely important for the translocation of the substrates and for the interaction between the proteasome and its regulatory complex. Instead of this N-terminal, the β-subunits have a pro-sequence, of different length, that is removed proteolitically during the assembling of the proteasome, making the internal cavity freely accessible. The analysis of data obtained from crystallographic studies of 20S proteasome in presence of its peptidic inhibitor, revealed that the active site of the complex was placed in the central cavity and each subunit had a fixed position whereas the interaction of the β subunits seemed to be essential for the expression of the proteolytic activity. The proteasome belongs to the family of the N-terminal nucleophil-hydrolase (Ntn-hydrolase): its catalytic center is constituted by a residue of N-terminal threonine present in β subunits that acts as nucleophile as well as proton acceptor, whilst other residues (Glu17, Lys33, Asp166) participate to the expression of the photolytic activities [63].

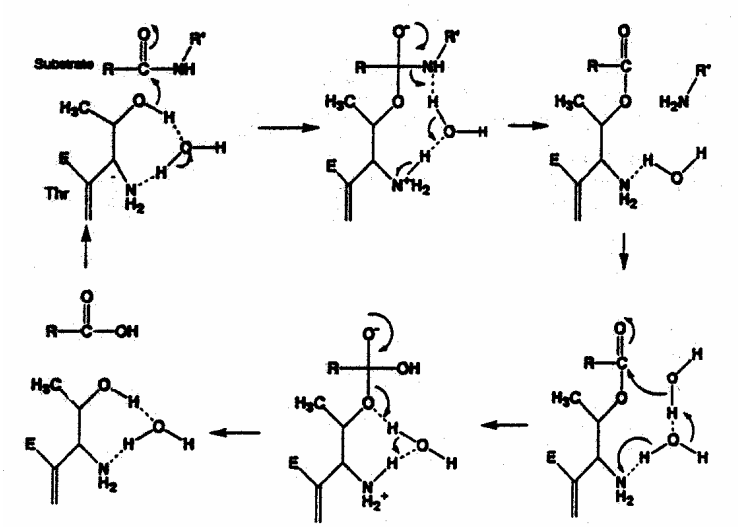

**Fig. 9:** Schematic representation of the catalytic mechanism of the proteasome 20S with the residue of threonine that acts as nucleophile and a molecule of water that acts as base.

### *Proteasome 20S - Function*

Five different hydrolasic activities were attributed to the 20S complex of mammalians, that can be characterized by the amino acidic residue involved in the bond cleavage [63,66,67].

According to this scheme, it is possible to identify:

- the chymotrypsin-like activity (ChT-L), preferentially cleaving the carboxylic side of aromatic residues
- the trypsin-like activity (T-L), preferentially cleaving the carboxylic side of basic amino acid residues
- the peptidil-glutamil-peptide hydrolasic (PGPH), preferentially cleaving the carboxylic side of acidic amino acidic residues
- the BrAAP (branched chain amino acid preferring) activity
- the SNAAP (small neutral amino acid preferring) activity

Each activity is associated to different β subunits, but the N-terminal threonine residues were reported only on 4 β subunits; thus, 3 of the 7 subunits were supposed not to possess any catalytic sites. Studies performed with irreversible inhibitors indicated that β subunits of mammalian proteasome (X,Y and Z), were associated respectively with the ChT-L, PGPH and T-L activities, whilst, it was not already clear whether the BrAAP and SNAAP activities were associated to one or more cooperating β subunits. The proteasome is not able to degrade *in vitro* denatured protein substrates, but it needs at to be activated by exposure to heat, by low

concentration of SDS or under particular ionic conditions. The molecular basis for these activating effects is far to be clear, but probably involves conformational changes in the proteasome (capable of opening and exposing the central cavity towards the outer side) and/or allosteric modifications of the catalytic site. This mechanism have a little physiological significance but it can mime the activity promoted by regulatory proteins, even if was not clear whether the direct activation of 20S by non protein factors happens in intact cells. Physiologically, the ubiquitin-proteasome complex is supposed to be involved in a number of cellular functions, like the cell growth and division, the degradation of regulatory cells like proto-oncogenes, the transcriptional factors and cyclines. In fact, it was showed that the proteasome-ubiquitin system regulates the activation of transcriptional factors NF-kB, involved in acute and chronic inflammatory responses, working as promoter and process amplifier. Moreover, in superior eukaryotes, the proteasome is involved in the presentation of antigens by the major complex of hystocompatibility of class I (MHC I), since it degrades proteins to small peptides of about 7-10 amino acids that, after being transferred to the endoplasmatic reticulum, are able to bind to MHC I molecules, creating a complex that is then transported on the plasmatic membrane and presented to cytotoxic lymphocytes T that precede cell disruption [68,69]. On the other hand, it was observed that under particular pathological conditions, cytokines can induce structural alteration on the proteasome, which in turn gains a higher efficiency in the process of antigen presentation. In fact, the induction by interferon γ in the cell of superior eukaryotes, leads to the appearing of three additional catalytically active β subunits (LMP2, MECL-1 and LMP7), that replace respectively the subunit Y, Z and X of the proteasome, thus yielding a complex known as immunoproteasome [70,71]. The immunoproteasome differs from the original one in the quaternary structure and consequently for its structural function, acquiring a capacity of cleaving more efficiently after hydrophobic and branched side chains residues, and less effectively after acidic residues. Among the functions of the ubiquitin-proteasome system, the degradation of oxidized cellular proteins is fundamental, since it provides to the proteasome itself a primary role in antioxidant defence mechanism and it seems to be able to act preferably at the level of hydrophobic residues, more exposed during the structural rearrangement of the oxidised protein. The selective degradation of proteins damaged by oxidation allows the cells to regenerate enzymes and proteins during normal aerobic life and to reduce the damage occurring during event of moderate oxidative stress. So, the proteasome constitutes an important defensive mechanism against aging process and the minimization of damages related to the rising of pathologies oxidation-induced.

# MATERIALS AND METHODS

## *Materials*

Bovine brain and thyme used for the purification of proteasome 20S, were obtained from local butcher. Substrates used to test ChT-L, PGPH and T-L activity (suc-LLVY-MCA and Z-GGL-pNA, Z-LLE-MCA and Z-LLE-2NA, Z-GGR-MCA and Z-GGR-2NA) were purchased from Sigma-Aldrich. Synthetic substrates (Z-LLR-2NA, Z-GPALG-pAB and Z-GPALA-pAB) used for testing the proteolytic BrAAP and SAAP activities of proteasome were kindly offered from Prof. M. Orlowski (Mount Sinai MedicaI School, New York). The aminopeptidase-N (Ap-N) necessary for testing this particular activity was purified following the Pfleiderer protocol and the subsequent modifications from Almenoff [72]. GroES (Chaperonine 10) was obtained from Sigma–Aldrich. All chemicals used were of the highest grade available. Superose 6 (HR 10/30) and Phenyl-Sepharose CL-4B (1.6 x 6.5 cm) chromatographic columns were obtained from Pharmacia. Carboxylate cuvettes and NHS Coupling Kit, containing N-hydroxysuccinimmide (NHS), 1-ethyl-3-(3-dimethylamino-propyl) carbodiimide (EDC), and ethanolamine were obtained from Affinity Sensors (UK). FPLC experiments were performed on an AKTA Chromatographic system obtained from Pharmacia-Amersham (Sweden). Kinetic and thermodynamic studies were performed on an IAsys plus device, Affinity Sensors (Cambridge, UK), obtained from ThermoFinnigan, Italy. Spectrophotometric assays were performed on a Varian Cary 1E spectrophotometric device (Palo Alto, California); fluorimetric assays were performed of a Shimadzu RF-5301PC spectrofluorophotometric device (Shimadzu Italia S.r.l.).

## *Methods*

### *Purification of 20S proteasome from thymus and from bovine brain*

The isolation and the purification of 20S proteasomes (MW 700kDa) from thymus and from bovine brain was performed according an experimental protocol developed by Eleuteri[73], based on a fractionation from 40 to 60% in ammonium sulphate, a ion exchange chromatography and two molecular exclusion chromatography that favour the removal of contaminants with low molecular weight. Higher purification rate is reached by addition of hydrophobic interaction chromatography in order to separate the 20S proteasome from the co-eluting chaperonin Hsp90.
For the purification of the MPC both from bovine brain and thymus, modifications were used in order to eliminate the phospholipidic constituents in tissues.

***Determination of protein content by Lowry method***

During early stages of purification, total protein content of different samples was evaluated by Lowry method[74], which assured a precise quantification also in fatty acid-containing samples. Samples were dissolved in water (250 µl) then added to 2.5 ml of a solution consisting of $Na_2CO_3$ 2% in NaOH 0.1 M (20 ml), $CuSO_4$ 1% (0.2 ml) and $NaOCO(CHOH)_2COONa$ 2% (0.2 ml). After 15 minutes, Folin reagent was added, and the resulting solution was incubated for 30 min. Protein content was assessed by comparison of the absorbance at 660 nm of the unknown samples with a standard curve built using known amounts of bovine serum albumin (BSA).

***Determination of the protein concentration through Bradford method***

The determination of the protein concentration of the cellular lysate, was obtained following Bradford method[75]. This assay allows the determination through by spectrophotometric absorbance at 595 of the complex proteins-Biorad reagent (100 mg/ml of Comassie Brilliant Blue G-250, ethanol and phosphoric acid). Since such absorbance is proportional to protein concentration, in order to know the concentration of the samples, it was necessary to make a calibration curve with known amounts of bovine serum albumin.

***Determination of Proteasomal Enzymatic Activities***

Chymotrypsin-like (ChT-L), Trypsin-like (T-L), peptidylglutamyl-peptide-hydrolyzing (PGPH), BrAAP (branched-chain amino acid preferring) and SNAAP (small neutral amino acid preferring) activities were measured using as substrate:

1) Cbz-Gly-Gly-Leu-PNA, concentration 0.4 mM in the assay, for the ChT-L activity;
2) Cbz-Leu-Leu-Glu-2NA, concentration 0.64 mM in the assay, for the PGPH activity;
3) Cbz-Leu-Leu-argon-2NA, concentration 0.4 mM in the assay, for the T-L activity;
4) Cbz-Gly-Pro-Ala-Leu-Gly-pAB, concentration 1 mM in the assay, for the BrAAP activity;
5) Cbz-Gly-Pro-Ala-Gly-Gly-pAB, concentration 1 mM in the assay, for the SNAAP activity.

The mixture of reaction was constituted by 10 µg of enzymatic protein (except for the measure of the BrAAP activity where 2 µg were used), the appropriate substrate for the activity that has to be measured (dissolved in DMSO) and TRIS-HCl buffer 0.05 M until a final volume of 250 µl. The samples were incubated at 37 °C for 60 minutes and the reaction was stopped by addition of an equal volume of 10 % trichloroacetic acid. The released chromophore group was then, measured by diazotization. For such purpose 500 µl of a sodium nitrite 0.1 % solution were added in order to promote the formation of the diazonium salt. The unreacted sodium nitrite was destroyed by addition of an excess of ammonium sulphammate. The final reaction of copulation

occurred between the salt of diazonium and N-1-naftiletilendiammine. Through a copulation reaction with N-1-naphthyl-ethylen-diamine, coloured compounds were then obtained having a maximum at 540 (pNA), 555 (pAB), and 580 nm (2NA). One unit of enzymatic activity was defined as the quantity of enzyme that catalyzed the release of 1 moles of chromophore group *per* hour. The specific activity is expressed in terms of unit for milligram of protein. In the case of the BrAAP and SNAAP activities, in order to get the aromatic amine free in solution, it has to be added to the mixture of reaction an excess of Aminopeptidase N (AP-N). In fact, since the proteasome promotes the hydrolysis of the binding between the amino acid in P2 and the one in P3 of this substrate, the AP-N is necessary in order to release the p-A group-at the last amino acid residue that is involved in the diazotization.

## *SPR BIOSENSING*

The anomalous diffraction on gratings due to the excitation of surface plasma waves was first described in the beginning of the twentieth century by Wood [76]. In the late sixties, optical excitation of surface plasmons by the method of attenuated total reflection was demonstrated by Kretschmann [77] and Otto [78]. Since then, surface plasmons have been intensively studied and their major properties have been assessed [79]. Surface plasmon resonance is a charge-density oscillation that may exist at the interface of two media with dielectric constants of opposite signs, for instance, a metal and a dielectric. The charge density wave is associated with an electromagnetic wave, the field vector of which reaches their maximum at the interface and decay evanescently into both media. This surface plasma wave (SPW) is a transverse-magnetic polarized wave. The propagation constant of the surface plasma wave propagating at the interface between a semi-infinite dielectric and metal is given by the following expression:

$$\beta = k\sqrt{\frac{\varepsilon_m N_s^2}{\varepsilon_m + N_s^2}} \qquad \textbf{(Eq.1)}$$

where $k$ denotes the free space wave number, $\varepsilon_m$ the dielectric constant of the metal ($\varepsilon_m = \varepsilon_{mr} + i\varepsilon_{mi}$), and $n_s$ the refractive index of the dielectric [79]. The SPW may be supported by the structure providing that $\varepsilon_{mr} < -N_s^2$. At optical wavelengths, this condition is fulfilled by several metals of which gold and silver are the most commonly used. Owing to high loss in the metal, the SPW propagates with high attenuation in the visible and near-infrared spectral regions. The

electromagnetic field of an SPW is distributed in a highly asymmetric fashion and the vast majority of the field is concentrated in the dielectric. An SPW propagating along the surface of silver is less attenuated and exhibits higher localization of electromagnetic field in the dielectric than an SPW supported by gold.

### *Concept of SPR optical chemical sensors and biosensors*

Generally, an SPR optical sensor comprises an optical system, a transducing medium which correlates the optical and chemical (or biochemical) domains, and an electronic system supporting the optoelectronic components of the sensor and allowing data processing. The transducing medium converts modifications in the quantity of interest into modifications in the refractive index which may be determined by optically interrogating the SPR. The optical part of the SPR sensor contains a source of optical radiation and an optical structure in which SPW is excited and interrogated. In the process of interrogating the SPR, an electronic signal is generated and processed by the electronic system. Major properties of an SPR sensor are determined by properties of the sensor's subsystems. The sensor sensitivity, stability, and resolution depend upon properties of both the optical system and the transducing medium. The selectivity and response time of the sensor are primarily determined by the properties of the transducing medium.

### *Surface plasmon resonance-sensing configurations*

As the propagation length of SPW is very limited, the sensing action is performed directly in the area where the SPW is excited by an optical wave. The optical system used to excite the SPW is simultaneously used for the interrogation of SPR. Therefore, the sensitivity of SPR sensors cannot benefit from increasing the interaction length of the sensor as it is common in sensors employing guided modes of dielectric waveguides. As follows from Eq. (1), the propagation constant of SPW is always higher than that of optical wave propagation in the dielectric and thus the SPW cannot be excited directly by an incident optical wave at a planar metal–dielectric interface. Therefore the momentum of the incident optical wave has to be enhanced to match that of the SPW. This momentum change is commonly achieved using attenuated total reflection (ATR) in prism couplers and optical waveguides, and diffraction at the surface of diffraction gratings (fig. 10).

As the excitation of SPW by optical wave results in resonant transfer of energy into the SPW, SPR manifests itself by resonant absorption of the energy of the optical wave.

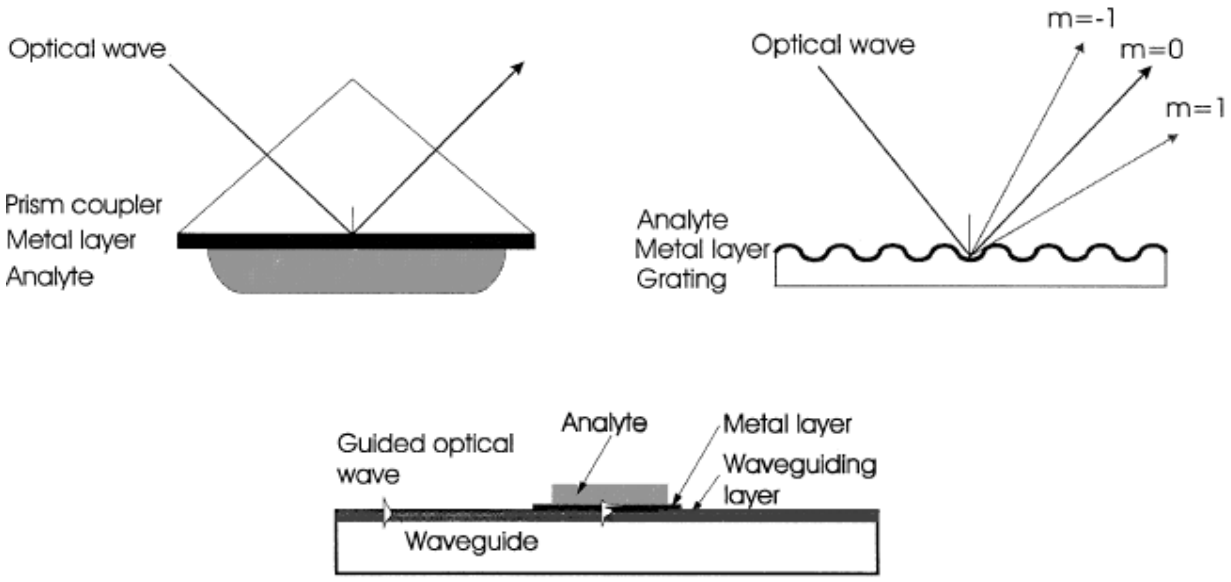


**Fig.10 :** Most common configurations of SPR sensors: prism coupler-based SPR system (ATR method); grating coupler-based SPR system; optical waveguide-based SPR system.

Owing to the strong concentration of the electromagnetic field in the dielectric (an order of magnitude higher than that in typical evanescent field sensors using dielectric waveguides) the propagation constant of the SPW, and consequently the SPR condition, is very sensitive to variations in the optical properties of the dielectric adjacent to the metal layer supporting SPW (transducing medium). Therefore, variations in the optical parameters of the transducing medium can be detected by monitoring the interaction between the SPW and the optical wave.

The following main detection approaches have been commonly used in SPR sensors:

1. measurement of the intensity of the optical wave near the resonance [80];

2. measurement of the resonant momentum of the optical wave including angular [81] and wavelength interrogation of SPR [82].

At present, approaches based on the measurement of the resonant momentum of the optical wave are prevalent primarily owing to the inherent simultaneous multiple data measurement which offers better signal to noise figures than simple intensity measurements.

Sensitivity of SPR sensors is defined as the derivative of the monitored SPR parameter (e.g. resonant angle or wavelength) with respect to the parameter to be determined (refractive index, thickness of a thin overlayer, concentration, etc.). The sensitivity of SPR-sensing devices has been widely studied. The sensitivity of SPR angular interrogation-based sensors to changes in the refractive index has been found to increase with decreasing operation wavelength, conversely, the sensitivity of SPR refractive index sensors using wavelength interrogation and

intensity measurement increases with the wavelength. In addition, SPR sensors based on wavelength interrogation and intensity measurement may benefit from using silver as an SPR active metal instead of gold [83]. The sensitivity of SPR sensors using ATR prism couplers is higher than that of SPR devices based on grating couplers. The sensitivity of SPR sensors to changes in the thickness of a thin overlayer, which is relevant to most SPR biosensors has been shown to follow essentially the same trends [84]. Sensor *resolution* is the minimum change in the parameter to be determined which can be resolved by a sensing device. The sensor resolution depends upon the accuracy with which the monitored SPR parameter can be determined by the specific sensing device and as such is limited by sensor system noise.

To illustrate the relationship between the sensor resolution and the accuracy with which the measured SPR parameter has to be determined, the sensor resolution has been calculated by dividing the assumed accuracy of the SPR parameter by the sensitivity of a particular detection approach. It should be noted that the accuracy with which the measured SPR parameter can be determined is very dependent upon the experimental circumstances and the degree of optimization of the particular sensor and therefore the ultimate resolution of the particular SPR sensor may differ from that of the considered model systems.

Another important parameter of an SPR sensor is its *operating range*, which is the range of values of the parameter to be determined, which can be measured by the sensor. While the operating range of intensity measurement-based SPR sensors is naturally limited due to the limited width of the SPR dip the operating range of angular and wavelength interrogation-based SPR sensors may be made much wider. In principle, the operating range of these sensors is determined by the detection system, more specifically by the angular or spectral range covered by the optical system-angular position detector array or spectrum analyzer, respectively. However, there is a trade-off between the dynamic range and resolution of these sensors. Inherently, the SPR method detects 'integral' changes in the refractive index in the vicinity of the surface supporting SPW and generally does not allow quantifying spatial distribution of the refractive index. While the effects of background refractive index variations can be effectively suppressed in multichannel SPR detection schemes, for the determination of the transducing medium refractive index spatial profile, the SPR method needs to be combined with another sensing technique which provides complementary information necessary for reconstructing the refractive index profile such as spectroscopy of guided modes in optical waveguides [85]. This method has been used for studying the process of diffusion of vapor molecules in a thin polymer layer [86]. The special problem of determining optical properties of homogeneous thin transparent films has been widely studied. Theoretically, the desired parameters of thin films may be

determined by fitting a single measurement of the angular reflectivity at a fixed wavelength. However, such a measurement requires very accurate data obtained on a well-characterized system to produce accurate results. The uncertainty in the determined parameters may be reduced by combining two sets of measurements which were obtained for different refractive indices of the superstrate or at different wavelengths [87].

***Fundamentals of surface plasmon resonance biosensors***

A surface plasma wave (SPW) or a surface plasmon-polariton is an electromagnetic wave which propagates along the boundary between a dielectric and a metal, which behaves like quasi-free electron plasma [88]. An SPW is a transverse-magnetic (TM) wave (magnetic vector is parallel to the plane of interface) and is characterized by the propagation constant and electromagnetic field distribution. The propagation constant of an SPW, β, can be expressed as:

$$\beta = \frac{\omega}{c}\sqrt{\frac{\varepsilon_M \varepsilon_D}{\varepsilon_M + \varepsilon_D}} \qquad \textbf{(Eq.2)}$$

where ω is the angular frequency, *c* is the speed of light in vacuum, and $\varepsilon_D$ and $\varepsilon_M$ are dielectric functions of the dielectric and metal, respectively. This equation describes an SPW if the real part of $\varepsilon_M$ is negative and its absolute value is smaller than $\varepsilon_D$. At optical wavelengths this condition is fulfilled for several metals of which gold is most commonly employed in SPR biosensors. The real and imaginary parts of the propagation constant describe spatial periodicity and attenuation of an SPW in the direction of propagation, respectively.

The electromagnetic field of an SPW is confined at the metal–dielectric boundary and decreases exponentially into both media. For an SPW at the boundary between gold and a dielectric with a refractive index of 1.32 the penetration depth (the distance from the interface at which the amplitude of the field falls to 1/*e* of its value at the metal surface) into the dielectric is typically 100–500 nm in the visible and near infrared regions[89].

***Concept of surface plasmon resonance biosensing***

Owing to the fact that the vast majority of the field of an SPW is concentrated in the dielectric, the propagation constant of the SPW is extremely sensitive to changes in the refractive index of the dielectric. This property of SPW is the underlying physical principle of affinity SPR biosensors – biomolecular recognition elements on the surface of metal recognize and capture analyte present in a liquid sample producing a local increase in the refractive index at the metal

surface. The refractive index increase gives rise to an increase in the propagation constant of SPW propagating along the metal surface (fig. 11) which can be accurately measured by optical means.

The magnitude of the change in the propagation constant of an SPW depends on the refractive index change and its distribution with respect to the profile of the SPW field.

There are two limiting cases:

1. Analyte capture occurs only within a short distance from the metal surface (fig. 11a).
2. Analyte capture occurs within the whole extent of the SPW field (fig. 11b).

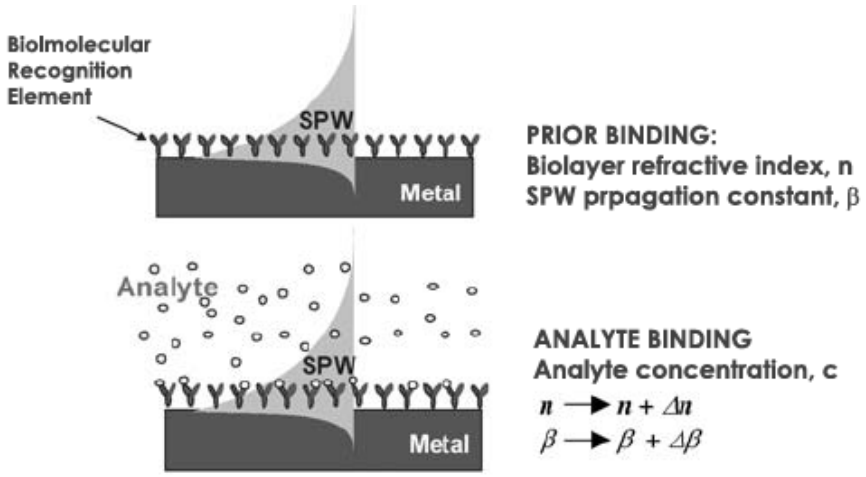


**Fig.11 :** Principle of SPR biosensing

Perturbation theory [90] suggests that if the binding occurs within the whole depth of the SPW field (fig. 5b), the binding-induced refractive index change, $\Delta n$, produces a change in the real part of the propagation constant, $\Delta\beta$, which is directly proportional to the refractive index change:

$$\mathrm{Re}\{\Delta\beta\} \cong k\Delta n \qquad \textbf{(Eq.3)}$$

where $k$ denotes the free-space wave number. If the refractive index change is caused by a binding event occurring within a distance from the surface $d$, much smaller than the penetration depth of the SPW, the corresponding change in the real part of the propagation constant can be expressed as follows:

$$\mathrm{Re}\{\Delta\beta\} \cong \frac{2n_s n_f k^2 d}{\sqrt{|\mathrm{Re}\{\varepsilon_m\}|}}\Delta n = Fk\Delta n \qquad \textbf{(Eq.4)}$$

where $n_f$ and $n_s$ denote the refractive index of the biolayer and the refractive index of the background dielectric medium (sample), respectively. The binding-induced change in the propagation constant of the SPW is proportional to the refractive index change and the depth of the area within which the change occurs. The factor $F$ ($F$<1) accounts for the fact that the interaction occurring within a thin layer is probed by only a fraction of the field of the SPW.

In SPR sensors, an SPW is excited by a light wave and the effect of this interaction on the characteristics of the light wave is measured. From these measurements, changes in the propagation constant of the SPW can be determined. Excitation of an SPW by light can occur only if the component of the light's wave vector that is parallel to the metal surface matches that of the SPW. This can be achieved by means of prism coupling, waveguide coupling, and grating coupling. In configurations based on prism coupling a light wave passes through a high refractive index prism and is totally reflected at the prism–metal layer interface generating an evanescent wave penetrating the metal layer (fig. 12a). This evanescent wave propagates along the interface with a propagation constant which can be adjusted to match that of the SPW by controlling the angle of incidence. This method is referred to as the attenuated total reflection (ATR) method [91]. The process of exciting an SPW in an optical waveguide-based SPR structure (fig. 12b) is similar to that in the ATR coupler. The light wave is guided by an optical waveguide and, when entering the region with a thin metal layer, it evanescently penetrates through the metal layer exciting an SPW at its outer boundary. Alternatively, an SPW can be excited by diffraction on a grating (fig. 12c). The component of the wave vector of the diffracted waves parallel to the interface is diffraction-increased by an amount which is inversely proportional to the period of the grating and can be matched to that of an SPW [92]. The interaction of a light wave with an SPW can alter light's characteristics such as amplitude, phase, polarization and spectral distribution. Changes in these characteristics can be correlated with changes in the propagation constant of the SPW. Therefore, binding-induced changes in the refractive index at the sensor surface and, consequently, the propagation constant of the SPW can be determined by measuring changes in one of these characteristics. Based on which characteristic is measured, SPR biosensors can be classified as angle, wavelength, intensity, phase, or polarization modulation-based sensors.

In SPR sensors with angular modulation the component of the light wave's wavevector parallel to the metal surface matching that of the SPW is determined by measuring the coupling strength

at a fixed wavelength and multiple angles of incidence of the light wave and determining the angle of incidence yielding the strongest coupling (fig. 13a). In SPR sensors with wavelength modulation the component of the light wave's wavevector parallel to the metal surface matching that of the SPW is determined by measuring the coupling strength at a fixed angle of incidence and multiple wavelengths and determining the wavelength yielding the strongest coupling (fig. 13b).

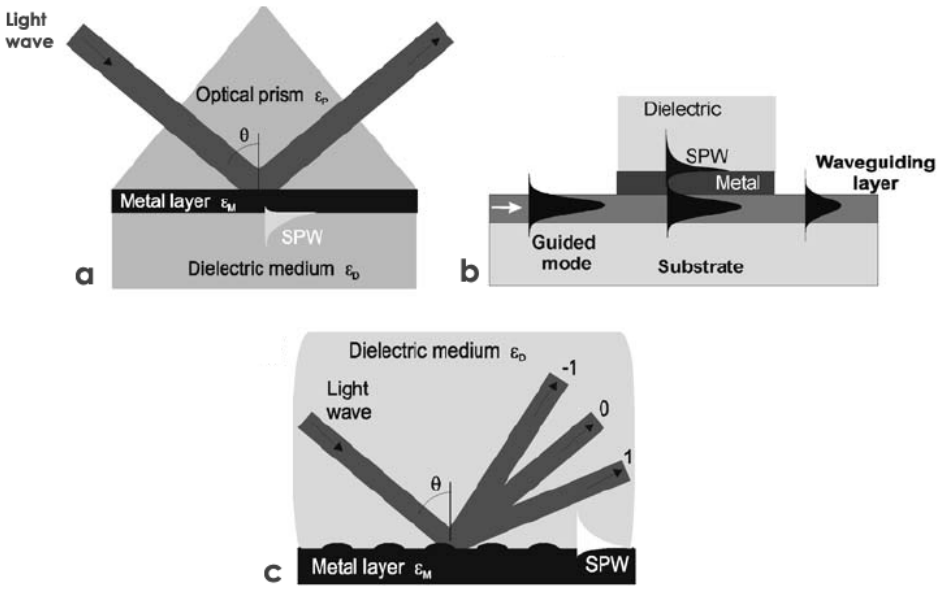


**Fig. 12:** Excitation of surface plasmon-polaritons: (**a**) by a light beam via prism coupling, (**b**) by a guided mode of optical waveguide, and (**c**) by light diffraction on a diffraction grating.

In SPR sensors with intensity modulation, the change in the intensity of the light wave interacting with the SPW is measured at a fixed wavelength and angle of incidence. In SPR sensors with phase modulation, shift in phase of the light wave interacting with the SPW is measured at a fixed wavelength and angle of incidence. In SPR sensors with polarization modulation, changes in the polarization are measured at a fixed wavelength and angle of incidence.

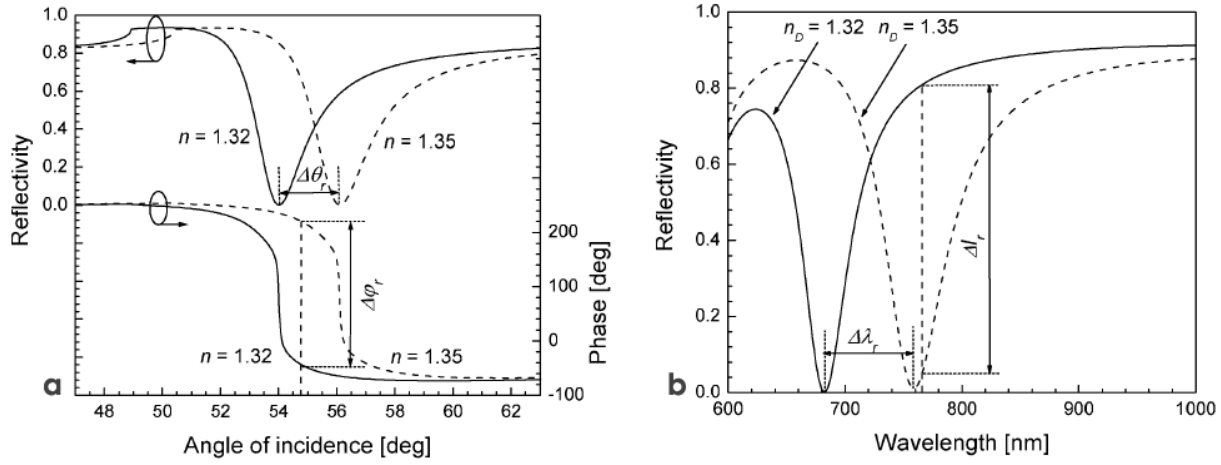


**Fig. 13:** Reflectivity and phase for light wave exciting an SPW in the Kretschmann geometry (glass prism – 50 nm thick gold layer – dielectric) versus (**a**) the angle of incidence for two different refractive indices of the dielectric (wavelength 682 nm), and (**b**) wavelength for two different refractive indices of the dielectric (angle of incidence 54°)

### *Performance characteristics*

The main performance characteristics relevant for SPR biosensors include sensitivity, accuracy, precision, repeatability, and the lowest detection limit. Sensor *sensitivity S* is the ratio of the change in sensor output, *P* to the change in measurand.

SPR biosensor sensitivity can be decomposed into two components – sensitivity to refractive index changes produced by the binding of analyte to biomolecular recognition elements on the sensor surface $S_{RI}$, and the efficiency *E*, with which the presence of analyte at a concentration *c* is converted into the change in the refractive index *n*:

$$S = \frac{\partial P}{\partial n}\frac{\partial n}{\partial c} = S_{RI}E \qquad \textbf{(Eq.5)}$$

The efficiency *E* depends on the properties of the biomolecular recognition elements and the target analyte. The refractive index sensitivity $S_{RI}$ can be decomposed into two terms:

$$S_{RI} = \frac{\partial P}{\partial \mathrm{Re}\{\beta\}}\frac{\partial \mathrm{Re}\{\beta\}}{\partial n} = S_1 S_2 \qquad \textbf{(Eq.6)}$$

The first term $S_1$ depends on the modulation method and the method of excitation of an SPW. The $S_2$ term is independent of the modulation method and the method of excitation of the SPW and describes the sensitivity of SPW's propagation constant to the refractive index change, Eq.3 and Eq.4. *Accuracy* describes the degree to which a sensor output represents the true value of the

measurand (analyte concentration). Accuracy is often confused with *precision* which refers to the way in which repeated measurements conform to them without a reference to any true value. *Repeatability* refers to the capacity of a sensor to reproduce output reading under the same measurement conditions over a short interval of time. The *lowest detection limit* describes the lowest concentration of analyte that can be measured by the sensor.

***SPR biosensing formats***

An interaction between a biomolecular recognition element on an SPR sensor surface and analyte in a liquid sample is governed by kinetic equations. In order to illustrate fundamental properties of the interaction, we shall discuss the pseudo-first-order kinetic equation:

$$\frac{dR}{dt} = k_a c(1 - R) - k_d R \qquad \textbf{(Eq.7)}$$

where $R$ is the relative amount of bound analyte, $c$ is analyte concentration, $t$ is time, and $k_a$ and $k_d$ are the association and dissociation kinetic rate constants, respectively [93]. This interaction model assumes 1:1 binding, rapid mixing of the analyte from the bulk phase to the sensor surface layer, and single-step binding. Observed binding, however, may deviate from this simple model due to more complex mechanisms of interaction and mass transport limitations. Eq. 7 yields for $R$:

$$R(t) = \left[ \frac{k_a c}{k_a c + k_d} - R_0 \right] \left(1 - e^{-(k_a c + k_d)t}\right) + R_0 \qquad \textbf{(Eq.8)}$$

where $R_0$ denotes the initial amount of analyte bound at the time $t$=0 [93]. Although SPR biosensors do not require the labelling of reactants, one of the binding partners has to be immobilized on the sensor surface. For the analysis of binding affinities and kinetics it is crucial that the measured binding reflects exclusively the native interaction of both reactants, i.e. that nonspecific surface-binding is negligible and that the immobilization does not affect the conformation of the binding site. Preferably, the macromolecule should be attached with uniform orientation and unrestrained accessibility for the mobile reactant. The sensor surface and the immobilization technique employed are therefore very important, and a number of different techniques have been described. Obviously, the best choice of which binding partner to immobilize and which immobilization technique to employ depends on the particular set of interacting macromolecules;

if possible, the comparative use of different techniques seems to be advantageous. The gold surface on the SPR sensor chip is usually covered with a self assembled monolayer of alkyl thiols. This suppresses non-specific binding and creates a hydrophilic surface. In most of the biosensor applications, sensor chips are used in which a matrix of carboxymethylated dextran is covalently attached (1-3 ng/mm$^2$) to form a flexible hydrogel of estimated thickness 100-200 nm or 220-400 nm. As is in the case with chromatographic matrices, this dextran matrix can be derivatized to give a number of different functional groups and to allow for a variety of immobilization chemistries. A regeneration procedure for this sensor chip has been described. The particular advantage of using this flexible, hydrophilic dextran matrix is that it provides better accessibility of the immobilized macromolecules to their binding and a potentially increased signal from the SPR sensor, by virtue of a relatively large number of immobilized biding sites and more efficient use of the evanescent field. A widely applied immobilization procedure utilizes activation of the carboxy groups of the dextran gel with a mixture of N-hydroxysuccinimide (NHS) and N-ethyl-N (dimethylaminopropill) carbodiimide to form NHS esters, which enables coupling to the amino groups on proteins. The effectiveness of the coupling relies on a pre-concentration of the protein by electrostatic attraction to the negatively charged matrix at pH values below the pI of the protein. However, it has been noted that this may lead to protein denaturation. Another disadvantage of the NHS-ester immobilization procedure is the potential occurrence of random coupling to different lysines on the protein, which may introduce subpopulations of binding sites with different accessibilities and reactivities. For these reasons, a variety of more specific immobilization methods have been described, such as coupling by thiol/disulfide exchange, aldehyde coupling, hydrazide group coupling, sulfhydryl group coupling, and chelate linkage of oligo-histidine tags. In several studies, for example, a specific orientation of the immobilized receptor domain was achieved by creating a thiol coupling/disulfide bond to cysteine residues that were introduced into one reactant via site-directed mutagenesis. For the immobilization of proteins with hydrophobic anchors, modification of the dextran matrix by heptyl residues has been described. Covalent linkage could be achieved though a perfluorophenylazide-derived hydrophobic crosslinker. Indirect coupling, exploiting the high affinity of the avidin-biotin interaction, can be achieved by immobilizing avidin/streptavidin to the dextran matrix and binding biotinylated macromolecules. This method has the additional advantage of not requiring pre-concentration in the matrix. It has been preferred for the immobilization of DNA and RNA but has also been generally used, for example, to immobilize lipid vesicles. The immobilization on aminosilane-derivatized surfaces (employing a resonant mirror biosensor) has been described. Alternatively, the use of mixed self-

assembled monolayers of functionalized alkyl thiols on the gold surface of the SPR biosensor has been demonstrated.

After successful immobilization of one of the reactants to the sensor surface, the real-time detection of local change in the refractive index at the sensor surface upon introduction of reactants into the mobile phase is a versatile tool for the study of reversible interactions.

***DATA ANALYSIS - A Model for a biomolecular interaction***

In a common model describing the interaction of an immobilized species E and a mobile macromolecule L, both reactants reversibly form a 1:1 complex EL, at a chemical on-rate constant for complex formation $k_{ass}$, and a chemical off-rate constant for complex dissociation $k_{diss}$. The thermodynamic equilibrium dissociation constant is then equal to

$$K_D = \frac{k_{diss}}{k_{ass}} \qquad \textbf{(Eq.9)}$$

Under ideal conditions, neglecting all potential complications due to the finite volume in which the reaction take place, and assuming that the concentration of the mobile reactant is held constant by an infinitely fast exchange with the bulk solution, the pseudo-first-order rate equation

$$\frac{d[EL]}{dt} = k_{ass}[L]([E]_{tot} - [EL]) - k_{diss}[EL] \qquad \textbf{(Eq.10)}$$

is valid, where [L] is constant and $[E]_{tot}$, denotes the total binding capacity of the surface on a molar basis. Usually, in a SPR biosensor experiment, relatively high concentrations of immobilized binding sites are required to produce a significant refractive index change upon binding. Therefore, the signal contribution of the free mobile reactant can usually be neglected. With the biosensor response R proportional to [EL], Eq. 10 gives:

$$\frac{dR}{dt} = k_{ass} f_0 R_{sat} - (k_{ass} f_0 + k_-)R \qquad \textbf{(Eq.11)}$$

where $f_0 \equiv [L]$, and $R_{sat}$ denotes the response at complete saturation of the immobilized binding sites. If no mobile reactant has been initially bound, the time-course of binding is described by an exponential

$$R(t) = R_{eq}(f_0)\left[1 - e^{-k_{obs}t}\right] \qquad \textbf{(Eq.12)}$$

with the observed rate constant

$$k_{on} = k_{ass} f_0 + k_{diss} \qquad \textbf{(Eq.13)}$$

approaching the equilibrium plateau signal

$$R_{eq}(f_0) = R_{\max}\left[1 + \frac{k_{diss}}{k_{ass} f_0}\right]^{-1} = R_{\max}\left[1 + \frac{K_D}{f_0}\right]^{-1} \qquad \textbf{(Eq.14)}$$

Equation 14 is equivalent to a Langmuir isotherm. If the free mobile reactant is removed from the buffer ($f_0 = 0$ for $t > t_0$), the complex dissociates exponentially with time:

$$R(t) = R(t_0)e^{[-k_{diss}(t-t_0)]} \qquad \textbf{(Eq.15)}$$

It should be noted that in this model the observed binding rate constant $k_{on}$ in the association phase is always higher than the chemical off-rate constant $k_{diss}$.

***Determination of Equilibrium Constants***

The thermodynamic equilibrium constant can be determined by the analysis of the dependence of the equilibrium plateau signals on the concentration of free mobile reactant using Eq. 14, or via measurement of the kinetic rate constants and using Eq.9. A very important advantage of the thermodynamic approach is that it does not require modelling of the biding progress and therefore is independent of mass transport influences. In the cuvette-based biosensor systems, equilibrium experiments may be performed employing a stepwise equilibrium titration procedure. The thermodynamic approach can also be applied for reactions that are too fast for a kinetic analysis. On the other hand, especially for slow reactions and small concentrations of mobile reactant, it may not be possible to reach equilibrium within the frequently limited time frame of an association experiment. In this case, the equilibrium analysis cannot be applied; however, the equilibrium response may be extrapolated on the basis of assumptions about the binding kinetics. Also, accurate determination of the equilibrium response can suffer from a signal offset due to a refractive index mismatch as a result of the buffer change and a

corresponding baseline offset ("bulk effect") or a baseline drift that might be caused by, for example, by temperature variations or nonspecific binding. However, this problem can be addressed using multiple cells and comparing the signal to that obtained in the absence of immobilized reactant. This can be particularly useful in the study of weak interactions, such as the binding of cell-adhesion molecules. Although the SPR measures surface binding, these competition experiments indirectly allow the determination of the affinity of E and L in solution. This enables diagnosis of the effects of immobilization. Also, such competitive experiments facilitate the detection of interactions with small reactants that would give an inadequate response in a direct SPR experiment. The kinetic variant of the competition analysis similarly can avoid problems resulting from mass transport and other factors confounding the interpretation of binding kinetics, if the biding rate constants $k_{on}$ are purely operationally defined. This approach can rely solely on their linear dependency on the concentration of free reactant L, or alternatively, a plot of the empirical dependence of $k_{on}[L]$ may serve as a calibration for the determination of the concentration of free reactant L. This variant of the competition experiment does not require the attainment of binding equilibrium.

***Analysis of Binding Kinetics***

The analysis of the kinetics of the interaction requires mathematical modelling of the binding-progress curves. For the simple 1:1 interaction, the pseudo-first-order kinetic exhibits a single exponential approach to the equilibrium signal (Eq. 12,15). Two different data analysis strategies have been proposed to extract the rate constants $k_{ass}$ and $k_{diss}$: linear regression of plots of dR/dt vs R for the association phase and $\ln[R(t_0)/R(t)]$ versus time for the dissociation phase; alternatively, a nonlinear fit with the integrated rate equations (Eq. 12,15) may be used. Although equivalent in principle, except for the more advantageous error distributions in the nonlinear regression, these strategies differ in their potential for ease of extension to account for the influence of mass transport, or for the presence of different subpopulations of binding sites respectively. A fit of Equation 13 to $k_{on}(f_0)$ obtained in a series of experiments at different concentrations of mobile reactant reveals both chemical rate constants $k_{ass}$ and $k_{diss}$. In practice, however, $k_{diss}$ may be poorly defined by this method, and therefore the analysis of the dissociation phase is advantageous. To account for artefacts of refractive index mismatch during the buffer change, the initial parts of the association and dissociation phases are usually excluded from the analysis. In combination with this adjustment, when nonlinear regression is used, a parameter for an unknown baseline, which in some studies may include baseline drift, is added to Equations 12 and 15. Since the experimental binding-progress curves often do not follow a

single exponential and can be best fit with double exponential expressions, the use of a model with two independent classes of immobilized binding sites has been proposed. This model allows for fitting the data with equations similar to Equations 12 and 15 but extended to a superposition of independent terms for each binding site. Similarly, a model for the interaction of two different mobile reactants competing for one class of immobilized binding sites leads to double exponential expressions, and has been proposed for use in kinetic competition experiments. Many bimolecular interactions might not follow simple pseudo-first-order binding kinetics. These analyses could, in principle, be performed by global analysis of data from a series of experiments obtained under a variety of different concentrations of mobile and immobile reactants. However, the practical limitations of the biosensor experiments appear to severely constrain this approach. It has been pointed out that mass transport limitation and related inhomogeneities within the sensor can appear as artefacts in the measured binding-progress curves, and that these can be similar to the results expected from more complicated binding schemes, such as apparently cooperative binding and multi-exponential binding. Nevertheless, at least some qualitative information about more complex binding schemes may be obtained. For example, experiments by Hausdorf [94] suggested the presence of a slow conformational change of one reactant.

***Possible Effects of the Immobilization***

The immobilization of reactants to the sensor surface can in some cases interfere with their binding properties by, for example, inducing conformational changes in the binding sites or sterically restricting the access of the binding partner. If nonspecific immobilization chemistry such as amine coupling is employed, multiple subpopulations of different orientations and different affinities could be produced. This should result in a broadening of the binding isotherm in the equilibrium data, while the binding kinetics could be characterized by multi-exponential binding-progress curves, each exponential term reflecting binding to a subpopulation of independent binding sites. Based on the empirical observation that single-exponential binding progress is often preserved at low concentrations of the mobile reactant, O'Shannessy and Winzor proposed restriction of the data analysis to those data that are in conformity with the description of simple 1:1 pseudo-first-order kinetics. These data contain the most information on the best accessible binding sites, which can be assumed to best mimic the affinity in solution. Significant binding to more restricted orientations of binding sites with correspondingly lower affinities takes place only at higher concentrations of mobile reactant. On the other hand, apparently multi-exponential binding can also be a result of mass transport limitations and non-

uniform distribution of the binding sites within the immobilization matrix. In this case, the experiments with low concentrations of mobile reactant would give kinetic curves that appear to be single-exponential, apparently in conformity with pure pseudo-first-order binding. However, the rate constants derived from these data could be orders of magnitude below the true intrinsic chemical rate constants. Therefore, this ambiguity of the interpretation should be resolved experimentally, by means of control experiments for mass transport limitations and for artefacts of immobilization. A different choice in the employed coupling chemistry, solution competition experiments, and the complete characterization of the binding isotherm by equilibrium experiments could be potentially useful tools. Another possible effect of the immobilization that is related to the high surface density of binding sites in biosensor experiments is that some immobilized macromolecules may have the potential for oligomerization. Whether binding properties change with the oligomeric state, or if the mobile reactant is multivalent, the results of a biosensor experiment may depend on the surface density of the immobilized species.

***Steric hindrance***

It has been noted that high local concentrations of immobilized reactant at sensor surface can lead to steric hindrance in binding to neighbouring sites. In several studies, high macromolecules concentrations of up to 100 mg/ml and more within the immobilization matrix would make steric hindrance and excluded-volume effects more than likely. In some respects, this would affect the binding process in a way similar to that of subclasses of differently accessible binding sites. Both lead to a broadening of the binding isotherm and have the smallest impact on the binding kinetics at low saturation of the binding sites. However, the measured dissociation rate can be expected to be less affected for the exc1uded-volume effect. Edwards et a1. [93] compared the binding kinetics of human serum albumin to an antibody immobilized either in a dextran matrix or on an aminosilane surface In the presence of the immobilization matrix, the data were well described by a double exponential, while the binding to the aminosilane-bound binding sites was described by a single exponential. Concluding that steric hindrance affected binding within the dextran matrix, the investigators interpreted the fast component of the binding progress as representative of binding events similar to those in solution; they interpreted the slow component as produced by artefacts of steric hindrance or restricted access to the binding sites. With the fast component identified as $k_{on}$ in Equation 13, a conventional analysis could be performed. However, high macromolecule concentrations also reduce the transport of the mobile reactant, and under transport limited conditions, it is the earlier part, and consequently the fast component, of the binding progress that is most influenced by a number of parameters not related to chemical

reaction rates. Therefore, again, experimental approaches seem to be superior to the analytical approach. A change in the density of immobilized binding sites can diagnose and eliminate the effects of steric hindrance. It should be noted that the direct attachment to a planar surface in the absence of an immobilization matrix done does not necessarily eliminate these problems, since the effects of excluded area might persist at high surface densities.

## *Fluorescence*

The luminescence phenomenon is defined as the spontaneous emission of radiation of electrically or vibrationally excited species not in thermal equilibrium with its environment.

The most well known form of luminescence is certainly those consequent to the absorption of light (photoluminescence), of which the most known is fluorescence. Less known is the chemiluminescence (CL), defined as the luminescence derived from an exothermal chemical process that brings to the formation of a product in an electronically excited state, that decades to the fundamental state by emitting photons. Inside the chemioluminscence, the bioluminescence (BL) it's always caused by a chemical process but happens in living organism and involves enzymes of photoproteins. The bioluminescence phenomenon is widely diffused in nature, both in acquatic organism like bacteria, algae, and fish and in land organism like fireflies and some species of worms and mushrooms.

On an chemical-analytical basis the luminescence represents a fundamental and versatile method for the developing of specific and sensible methodologies, with wide applications in biomedicine, biotechnology, molecular biology, pharmacology and in agro and food chemical. For instance, systems based on chemioluminescence methods almost fully replaced radioisotopes, like $^{3}H$ and $^{125}I$, widely used for more than 30 years in clinical chemistry for the labelling and the preparation of tracing molecules. Historically, the photoluminescence, and fluorescence in particular, have represented the first analytical methodology with high revealability. Several fluorophores have been developed and applied in several chemistry sectors: for instance, fluoresceine is widely used in immunochemistry field.

### *General principles of fluorescence*

As all other spectroscopic techniques, fluorescence studies the interaction between the electromagnetic radiation and matter [87-88]. The electromagnetic radiation is characterized by its frequency (or wavelength), by the intensity and polarization. The frequency (cycles *per* second) determines the energy of the photons associated to the radiation; the intensity express the numbers of photons emitted *per* time unit by the source of the radiation multiplied for the

energy of each photon, and then the flow of energy *per* time unit; the polarization is defined as the direction of the vibration of electrical and magnetic field vectors associated to the radiation.
A key feature of the electromagnetic radiation is the wave-particle dualism. In fact, it can act as discrete packets of energy (namely photons), whose energy is determined by the frequency of the radiation:

$$E = h\nu = hc / \lambda \qquad \textbf{(Eq.16)}$$

Where $h$ is the Plank constant and $c$ is the speed of light.
The interaction between the electromagnetic radiation and matter causes an energetic transition between ground and excited states of the target molecule. This energy transfer can be revealed through the decrease in the radiation intensity. Emission is related to an energy loss of the system, after the electronic transition from the excited state to a ground one, producing an electromagnetic radiation. While the absorption phenomena are always associated to an increase of molecular energy, the decrease of the molecule energy not necessarily involves emission, since energy can be dissipated in different pathways. Generally, the most common process of energy dissipation is thermal relaxation due to the molecular movements. The entity of such energy loss depends upon a number of factors, related to the molecular characteristics of the system (magnitude, rigidity and shape), and to external factors, as the presence of solvents or other solutes.
After an energetic transition between the ground state and an excited state of a molecular system, there is a competition between the processes of thermal relaxation e ri-emission of magnetic radiation that determines the fluorescence effect.
The efficiency of non-radiatives processes depends strongly on the surrounding environment, like the intensity of ri-emitted radiation (fluorescence). Because of these features, the fluorescence can be considered as a technique highly sensible to changes in the fluorophore surrounding environment and consequently to the conformational changes in a macromolecular system.
Absorption and emission phenomena are well represented in the diagram of energetic levels proposed by Jablonski (fig.14).
The ground state is indicated with $S_0$, whereas those with higher energy are referred to as $S_1$, $S_2$, $S_3$, … $S_n$, respectively. The transition between states is represented by vertical lines, corresponding to absorbance or emission of light. In a fluorophore, the absorbance of light energy induces the promotion of an electron to one of the vibrational excited levels ($S_1$ or $S_2$).

The molecules at this point may relax rapidly to reach the lowest vibrational level of the S state. This process, that take place in a relative short period of time ($10^{-12}$ s), is called internal conversion (IC) and it completes before the emission of fluorescence that has time order of $10^{-8}$ s. The return is reached by returning to an excited vibrational state of the ground electronic state, evolving rapidly through equilibrium.

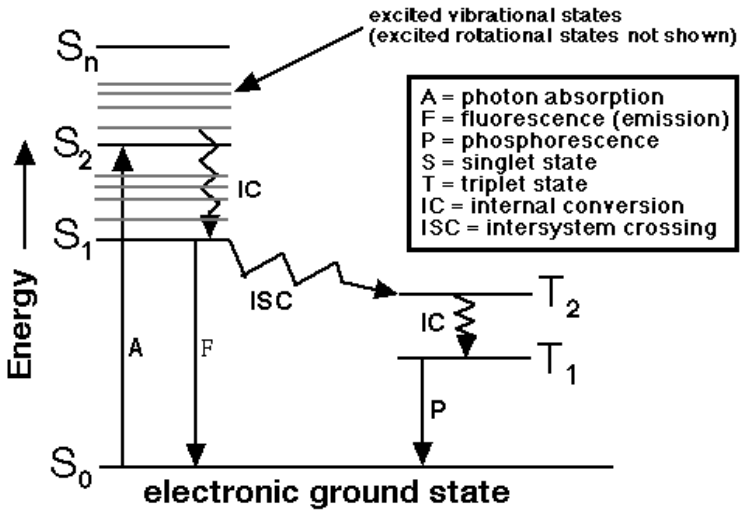


**Fig. 14:** Jabłonski diagram

The molecules in state $S_1$ can finally shift to a triplet state ($T_1$) through a spin inversion. The emission from the T state is called phosphorescence and is generally shifted towards higher wave lengths (lower energy) respect to fluorescence. The conversion from $S_1$ to $T_1$ state is defined intersystem crossing (ISC). The transition from the $T_1$ to the ground singlet state is forbidden, and as a consequence, the resulting velocity for the triplet is of several folds lower in comparison with the singlet.

The analysis of Jabonski diagram reveals that the emitted energy is lower than absorbed energy, so the fluorescence phenomena take place at lower energies (bathochromic shift), corresponding to higher wave lengths[95,96].

This phenomenon was observed for the first time by sir G.G.Stokes in 1852 at Cambridge University[97].

The cause of this phenomenon (namely Stoke's shift) (Fig.15), is a rapid decrease to lowest vibrational of the $S_1$ state. In addiction further Stoke's shift can be caused by solvent, collision between molecules and temperature.

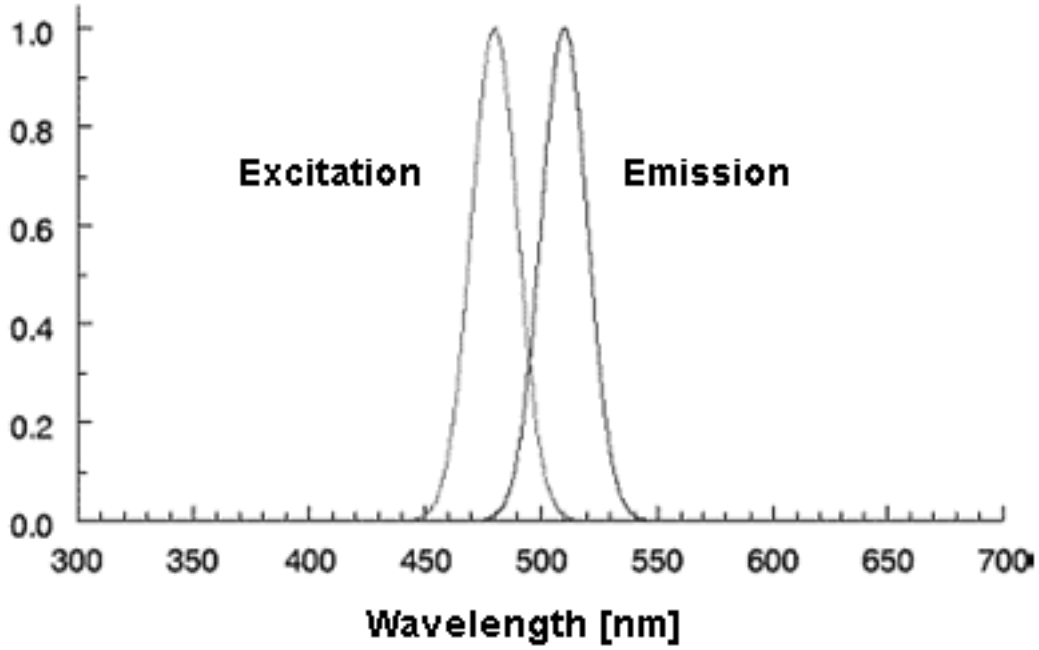


**Fig. 15:** Excitation and emission spectra for a fluorophore. Relative *Stoke's shitf is reported.*

***Luminescent Biosensors***

In biochemistry, fluorophores can be divided into two separate classes:

- intrinsic, present in some proteins and for this reason they act as natural emission substances
- extrinsic, to be added to the sample in order to obtain fluorescence.

Among the intrinsic fluorophores, we can find the aromatic aminoacids, like tyrosine, phenylalanine and tryptophan, the reduced form of the cofactor NADH, the oxidised form of the cofactor FAD, chlorophyll, etc.

Among proteins, the fluorophore dominating group is the indole of the tryptophan, absorbing near to 280 nm and emits near to 340 nm. In DNA and lipids, the intrinsic fluorescence is not intense enough to be able to conduct particular experiences. Some proteins may need to be traced with chromophores that can have an excitation or emission wavelength higher than those of amino acids.

Fluorophores able to form covalent or non-covalent bonds with proteins are numerous and may possess reactive groups able to link to N-groups and to S-groups of proteins.

The most frequently used probes are tetramethylrodamine, 5-isotiocyanate (TRITC), fluoresceine 5-isotiocyanate (FITC), 5-(iodoacetamide) fluoresceine (5-IAF), dansyl chloride (DNS-Cl), 5-dimethylamino-1-naphtalensulfonylchloride, 6-acryloil-2-dimethylaminonapthalene (Acrylodan) and some domanine derivatives like Texas Red Sulfonyl Chloride and Lisamine Rhodamine B Sulfonyl Chloride. Among those, Dansyl-Chloride was widely used for biochemical analysis. Dansyl-Chloride can be excited at 350 nm (where proteins do not absorb) and emit at 520 nm. It also has a convenient time life (10 ns) and it is highly sensible to the polarity of the solvent.

The fluoresceine and the rodamine are also widely used as extrinsic probes: they absorb at favourable wavelengths (480 nm and 560 nm, respectively and are characterized by molar extinction coefficients of 80.000 $M^{-1}$ $cm^{-1}$). In order to be used as biological markers, fluorescent probes are functionalized with reactive groups like iodoacetamides, isothiocianates and maleimides that are able to react selectively with other functional groups of the biomolecules. Iodoacetamides and malimides groups are able to react with sulphur groups, while the isothiocyanate, N-hydroxysuccinimide and sulfonylchloride are able to link to amino groups[98].

As an example, the dansyl chloride and the fluoresceine isothiocyanate react with the amino groups of proteins, and so the fluorescent part provokes the marked molecule to emit in the blue and green spectrum zone, respectively. One of the problems of organic fluorophores is their tendency to of self-quenching: this phenomenon can happen if several fluoresceine molecules linked to the protein are close enough (40Å) to make an energy transfer from one molecule to another. This process is possible since the fluoresceine is subject to a minor Stoke's shift. For this reason the study of biological markers is redirected towards molecules that may present significative Stoke's shift.

***Fluorescence lifetimes and Quantum Yields***

Fluorescence lifetimes and quantum yields of fluorescent substances are frequently measured. The meanings of these parameters are best illustrated by reference to a modified Jablonski diagram (Fig. 16). In this diagram we did not explicitly illustrate the individual relaxation processes leading to the relaxed $S_1$ state. Instead, we direct increased attention to those processes responsible for return to the ground state. In particular, we are interested in the emissive rate of the fluorophore (r) and its rate of radiationless decay to $S_0$***(k)*****.**

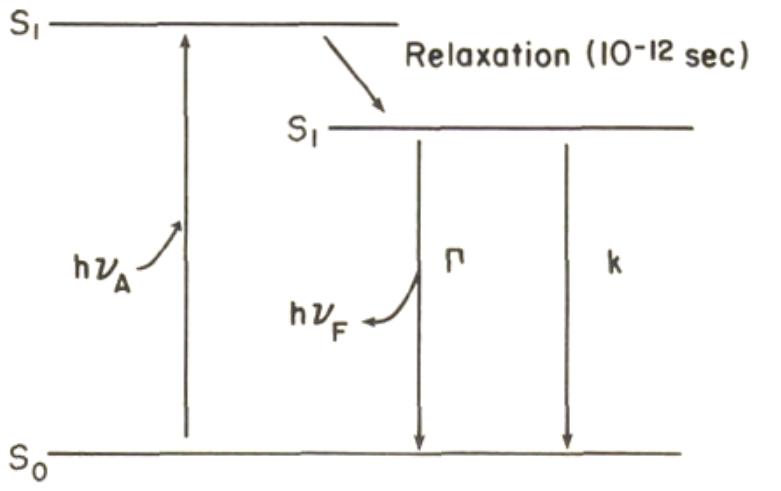


**Fig. 16:** Modified Jablonski diagram

The fluorescence quantum yield is the ratio of the number of photons emitted to the number absorbed. The rate constants $\Gamma$ and $k$ both depopulate the excited state. The fraction of fluorophores which decay through emission, and hence the quantum yield, is given by

$$Q = \frac{\Gamma}{\Gamma + k} \qquad \textbf{(Eq.17)}$$

The quantum yield can be close to unity if the radiationless rate of deactivation is much smaller than the rate of radiative decay, that is k << $\Gamma$**.** We note that the energy yield of fluorescence is always less than unity because of Stokes' losses. For convenience we have grouped all possible nonradiative decay processes with the single rate constant $k$. The lifetime of the excited state is defined by the average time the molecule spends in the excited state prior to return to the ground state. Generally, fluorescence lifetimes are near 10 nsec. For the fluorophore illustrated by Figure 16 the lifetime is

$$\tau = \frac{1}{\Gamma + k} \qquad \textbf{(Eq.18)}$$

One should remember that fluorescence emission is a random process, and few molecules emit their photons at t = $\tau$**.** The lifetime is an average value f the time spent in the excited state. For a single exponential decay (Chapter 3) 63% of the molecules have decayed prior to t = $\tau$ and 37%

decay at t > $\tau$. The lifetime of the fluorophore in the absence of nonradiative processes is called the intrinsic lifetime, and is given by

$$\tau_0 = 1/\Gamma \qquad \textbf{(Eq.19)}$$

This leads to the familiar relationship between the quantum yield and the lifetime

$$Q = \tau/\tau_0 \qquad \textbf{(Eq.20)}$$

The quantum yield and lifetime can be modified by any factors which affect either of the rate constants. For example, a molecule may be nonfluorescent as a result of a large rate of internal conversion or a slow rate of emission. Scintillators are generally chosen for their high quantum yields. These high yields are a result of large $\Gamma$ values. Hence, the lifetimes are generally short, near 1 nsec. The fluorescence emissions of aromatic substances containing $-NO_2$ groups are generally weak, primarily as a result of large values for *k*. The quantum yields of phosphorescence are extremely small in fluid solutions at room temperature. The triplet-to-singlet transition is forbidden by symmetry, and the rates of spontaneous emission are about $10^3$ $sec^{-1}$ or smaller. Since *k* values are near $10^9$ $sec^{-1}$, quantum yields of phosphorescence are small at room temperature. From equation (17) one can predict phosphorescence yields of $10^{-6}$.

## *Fluorescence Anisotropy*

Fluorophores preferentially absorb photons whose electric vectors are aligned parallel to the transition moment of the fluorophore. The transition moment has a defined orientation to the fluorophore. In an isotropic solution, fluorophores are molecules orientated randomly. Upon excitation with polarized light, only fluorogenic molecules whose absorption transition dipole is parallel to the electric vector of the excitation are selectively excited. The selective excitation of a partially oriented population of fluorophors results in a partially polarized fluorescence emission. The transition moments for absorption and emission have fixed orientations within

each fluorophore, and the relative angle between these moments determines the maximum measured anisotropy.

Fluorescence anisotropy measurements have been widely used to detect change in the rotational diffusion properties of many proteins. This method has been applied to quantify protein-protein association reaction. The investigated protein is initially labelled with a fluorophore with appropriate fluorescence lifetime. The sample is then excited with vertically polarized light. The value of anisotropy (r) is calculated by determining intensity of the horizontally and vertically polarized emission light by using Eq. (21):

$$r = \frac{(I_V - B_V) - G(I_h - B_h)}{(I_V - B_V) + 2G(I_h - B_h)} \qquad \textbf{(Eq.21)}$$

where $I_V$ ,$I_h$ , and $B_h$ are the intensities of the vertically and horizontally polarized emissions of sample ($I$) and blank ($B$) with vertically and horizontally polarized excitation light. $G$ is a correction factor equal to $I_V/I_h$, where the excitation light is horizontally and vertically polarized[99,100]. The relationship between anisotropy and rotation diffusion of the particle carrying the fluorophore is described by the Perrin-Weber equation:

$$\frac{r_0}{r} = 1 + \frac{R_g T}{\eta V}\tau \qquad \textbf{(Eq.22)}$$

where $r$ is the measured anisotropy, $R_g$ *is the* gas constant, $\tau$ is the lifetime of the excited state, $\eta$ is the viscosity of the solution, and $V$ is the effective volume of the particle carrying the fluorescent probe. This law predicts a linear relationship between $1/r$ and the ration $T/\eta$. The intercept of $1/r$ vs $T/\eta$ on the ordinate determines $r_0$, the anisotropy should, in principle, only be a function of the fluorophore. Assuming that fluorophore-labelled ligand can exist in either the free (f) or the bound (b) form, the final value of the observed anisotropy can be described as

$$r = f_f r_f + f_b r_b \qquad \textbf{(Eq.23)}$$

where $r_f$ and $r_b$ refer to the anisotropies of the free and bound fluorophore-labelled compound, respectively; $r$ is observed anisotropy value; and $f_f$ and $f_b$ refer to the fraction of the total fluorescence that is generated by free and bound fluorophore-labeled compound, respectively ($f_f + f_b = 1$). Equation 23 is correct when the quantum yield of the fluorophore is not affected

owing to the protein-protein interaction. The $r_f$ and $r_b$ values can be easily measured by examining the fluorophore-labelled ligand in the absence of the protein and under conditions of complete binding (high protein concentration), respectively. Equation 23 can be rearranged to yield

$$f_b = \frac{r - r_f}{r_b - r_f} \qquad \textbf{(Eq.24)}$$

allowing one to analyze quantitatively the ligand-protein interaction.

# EXPERIMENTAL

***Isolation and purification of the bovine brain multicatalytic protease***

In order to isolate and purify the bovine brain multicatalytic protease complex, bovine brain was previously washed in physiological solution and the external membrane was removed; then the grey substance was separated from the white and contemporarily fat and fibrous parts were removed. The isolated grey substance, 235 g, was initially homogenised with Waring-Blendor in Tris-HCl 50 mM, KCl 150 mM, EDTA 2 mM, pH 7.5 buffer (ratio 1:2.5 tissue/buffer). The collected suspension was again homogenised with a Potter-Elvejham system. Mentioned operations were carried out at 4°C. In order to help the extraction, the homogenate was kept overnight in ice under mild stirring. After a 13500 x g centrifugation x 1h, the surnatant was added with solid ammonium sulphate up to a 40% - 60% salt saturation. The precipitate was suspended in Tris-EDTA 50 mM + KCl 150 mM, pH 8.3 buffer, and dialysed with the same buffer overnight. Then, a first separation was carried out by gel-filtration on a Sephacryl S200 column, equilibrated with Tris-EDTA 50 mM, KCl 150 mM a pH 8.3 buffer. This step removes a major part of phospholipids. Proteasome fractions were identified on the basis of their chymotropism-like activity, than collected and concentrated by ultra filtration (YM10 membrane) under nitrogen atmosphere.

The concentrated sample was loaded on a DEAE-Sephacel column, equilibrated with Tris-EDTA 50 mM, pH 7.5 buffer and eluted in KCl (0-0.8 M) linear gradient. The active fractions were collected and dialysed in Tris-EDTA 50 mM, KCl 150 mM, pH 7.5 buffer, concentrated and loaded on a Superose 6 FPCL column. The gel-filtration eluted peak was again loaded on a Phenyl Sepharose CL/4B FPLC column, equilibrated in Tris-EDTA 20 mM, $(NH_4)_2SO_4$ al 30%, pH 7.5 buffer and eluted in an ammonium sulphate (30%-0%) linear gradient.

The results of SDS-PAGE (12% polyacrylamide) are shown in figure 17. The MPC characteristic electrophoregram presents 10 protein bands with molecular weights ranging between 21 and 32 kDa.

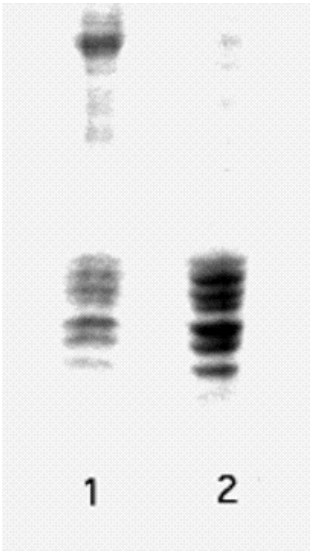


**Fig. 17 :** Poliacrilammide (12%) gel electrophoresis carried out in denaturing conditions, after Superose 6 elution (lane 1) and after Phenyl Sepharose CL/4B elution (lane 2)

All quantitative data related to the bovine brain 20S proteasome purification steps are reported in table 1.

| **Purification step** | **volume (ml)** | **Protein (mg/ml)** | **Total activity** | **Spec. act. (U/mg)** | **recovery %** | **Purific. index** |
|---|---|---|---|---|---|---|
| homogenate | 780 | 80.7 | 969.6 | 0.015 | 100 | 1 |
| surnatant | 612 | 4.8 | 146.9 | 0.05 | 15.15 | 3.33 |
| $(NH_4)_2SO_4$ precipitation | 28 | 14.4 | 30.94 | 0.077 | 3.19 | 5.13 |
| Sephacryl S200 | 38 | 1.4 | 13.9 | 0.26 | 1.4 | 17.3 |
| DEAE-Sephacel | 126 | 0.39 | 10.71 | 0.21 | 1.1 | 14 |
| Superose 6 | 5,5 | 0.91 | 1.22 | 0.24 | 0.126 | 16 |
| Phenyl Sepharose | 7 | 0.17 | 1.64 | 1.35 | 0.17 | 90 |

**Tab 1:** Bovine brain 20S proteasome purification scheme

All the purification steps were carried out at ≤ 4° C. The protein concentration was measured with the Lowry method [74] for the first four steps**,** and with the Bradford method for the following steps. The chymotrypsin-like activity was measured as described in Materials and

Methods. Table 2 shows the specific activity of the proteolytic components of the bovine brain purified MPC.

| Component | Substrate Conc. (mM) | Specific activity (μmol/mg/h) |
|---|---|---|
| **BrAAP** | Z-GPALG-pAB (1.0) | 1.24 |
| **PGPH** | Z-LLE-2Na (0.64) | 1.53 |
| **ChT-L** | Z-GGL-pNA (0.4) | 3.60 |
| **T-L** | Z-LLR-2Na (0.4) | 0.42 |
| **SNAAP** | Z-GPAGG-pAB (1.0) | 0.55 |

**Tab 2 :** Bovine brain MPC proteolytic activity

***Isolation and purification of the bovine thymus multicatalytic protease***

The bovine thymus protease purification procedure has been similar to that one previously described bovine brain isolation. In details, 270 gr. of tissue, after the accurate fat removal, were firstly homogenised with a Waring-Blendor in Tris-HCl 10 mM, pH 7,5 buffer, than centrifuged at 13500 x g per one hour. The collected surnatant was added with 1% final streptomycin solution, in order to precipitate nucleic acids and nucleo-proteins. Then, the precipitate was added with solid ammonium sulphate up to a 40% - 60% salt saturation; it was suspended in Tris-EDTA 10 mM, pH 7.5 and dialysed in the same buffer.

Then, the sample was loaded on a DEAE-Sephacel column, equilibrated in Tris-EDTA 10 mM, pH 7.5 buffer and eluted with a 0.01- 0.5 M Tris-EDTA linear buffer. The following steps were two gel filtrations: the first on a Sephacryl S 300 column equilibrated and eluted with Tris-EDTA 250 mM, pH 8.3 buffer, the second on a Superose 6 equilibrated and eluted with Tris-EDTA 150 mM, pH 7.5 buffer. Figure 18 reports the SDS electrophoresis results of the Superose 6 eluted fraction, exhibiting the higher chymotrypsin-like activity.

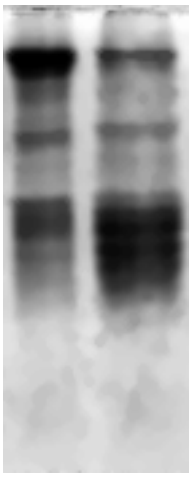


**Fig.18:** 12% (PAGE) polyacrilamide gel electrophoresis, in denaturing conditions, before (lane1) and after (lane 2) the Superose 6 chromatography. The electrophoresis was carried out according to the Laemmly[101] procedure.

Table 3 shows the results of the immunoproteasome purification steps, while Table 4 shows the specific activities of the five proteolytic components of the enzyme.

| **Purification steps** | **Volume (ml)** | **Protein (mg/ml)** | **Total activity** | **Spec. Act. (U/mg)** | **Recovery %** | **Purific. index** |
|---|---|---|---|---|---|---|
| homogenate | 1040 | 7 | 655 | 0.09 | 100 | 1 |
| surnatant | 740 | 1.3 | 510 | 0.53 | 77.9 | 5.9 |
| $(NH_4)_2SO_4$ precipitation | 69 | 2.62 | 257 | 1.42 | 39.2 | 15.8 |
| Sephacryl S200 | 222 | 0.50 | 231 | 2.08 | 35.3 | 23.1 |
| DEAE-Sephacel | 61 | 0.90 | 132 | 2.4 | 20.1 | 26.6 |
| Superose 6 | 46 | 0.90 | 95.2 | 2.3 | 14.5 | 25.5 |

**Tab. 3 :** Bovine thymus MPC purification scheme

The protein concentration was measured with the Lowry method [74] for the first 3 steps**,** and with the Bradford method for the remaining steps. Proteolytic activities have been measured according to Materials and Methods.

| Component | Substrate conc. (mM) | Specific activity (μmol/mg/h) |
|---|---|---|
| **BrAAP** | Z-GPALG-pAB (1.0) | 40.23 |
| **PGPH** | Z-LLE-2NA (0.64) | 0.80 |
| **ChT-L** | Z-GGL-pNA (0.4) | 1.04 |
| **T-L** | Z-(D)ALR-2NA (0.4) | 1.07 |
| **SNAAP** | Z-GPAGG-pAB (1.0) | 0.75 |

**Tab. 4 :** Thymus MPC proteolytic activities

## *Fluorimetric assays*

### *GroES labelling with Dansyl Chloride*

GroES (1mg/ml) was dialyzed overnight against 0.1 M carbonate buffer, pH 9.5, to remove any trace of Tris-HCl and ammonium sulphate. A slight molar excess of dansyl chloride was added to the protein solution, and the mixture is incubated at room temperature for 2 h in a dark tube. The solution is then dialyzed against 50 mM Tris-HCl, pH 7.8, a 4°C to remove any unbound dansyl chloride[102]. To quantify the amount of label bound to GroES, the concentration of dansyl chloride was measured by determining the absorbance of the sample at 339 nm, assuming 3378 $M^{-1}$ $cm^{-1}$ as the molar extinction coefficient. The protein concentration is measured as stated above. The final value is determined by the ratio of the molar concentration of dansyl chloride label to the molar concentration of GroES oligomer.

### *GroES Binding to 20S proteasome from thymus and from bovine brain*

The GroES (120 nM) labelled with dansyl chloride has been incubated with increasing quantity of proteasome from thymus and from bovine brain (30 nM- 150 nM) in 50 mM Tris-HCl pH 7.8. After 10 min. of pre-incubation, for anisotropy measurements, the samples were excited at 374 nm and the emission was measured at 480 nm. Each measurement was the average of 6 readings.

## *Biosensor studies*

The chemistry of immobilization most commonly used in protein application is coupling between carboxyl groups of carboxymethyl-dextrane and the amino primary groups of proteins

(N-terminal groups and lysine), through the EDC chemistry (1-ethyl-3-(3-dimetinaminopropil)carbodimmide) and NHS (N-hydroxysuccinimmide). This approach is also applicable to non-proteic biomolecules containing primary amino groups.

The electrostatic absorbance of the biomolecule on the carboxylate matrix depends on its concentration in solution; the level of this dependence and the interval of pH where it happens depend on the isoelectric point of the molecule that has to be immobilized.

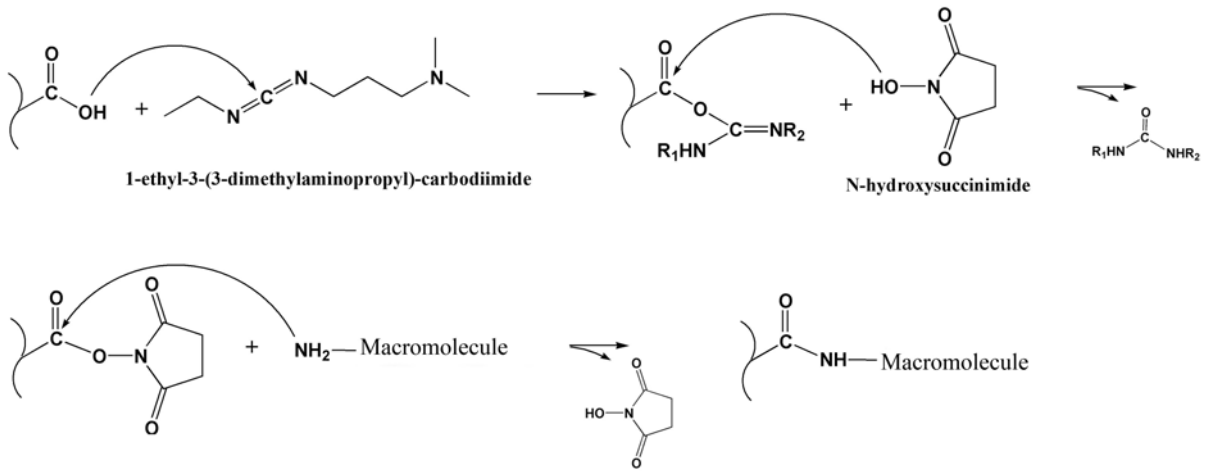


**Fig. 19:** Chemistry of immobilization of a macromolecule over carboxylate through EDC-HNS

### *Immobilization of GroES on Carboxylate Cuvette*

A carboxylate cuvette was inserted into the IAsys Biosensor and equilibrated at 25°C. The reaction chamber was always vibrostirred using a stirrer installed into the sensing chamber. Any impurity in the cuvette cells was removed by washing three times with 75 µl of PBS-T (10 mM sodium phosphate, 2.7 mM potassium chloride, 138 mM sodium chloride, containing 0.05%$_{(v/v)}$ Tween 20). Binding was measured at 5 sec intervals, and the readout from the biosensor was in arc-seconds units, which correspond to the accumulation of mass within the optical window at the binding surface. Each binding reaction was routinely followed for 4 min. Before the surface activation, the cell was washed with PBS (10 mM sodium phosphate, 2.7 mM potassium chloride, 138 mM sodium chloride) to wash out the detergent, which can cause a "mask" effect of the reactive groups. The cell was washed again with PBS, and a buffer baseline was recorded for 5 min (fig. 20, a-b). Immediately before use, equal volumes of NHS and EDC solutions were mixed to make up the activation mixture[103].

The PBS buffer was replaced with EDC/NHS activation mixture and incubated for 7 min to activate the carboxylic groups on the surface (fig. 20, c). The activation mixture was removed by

washing with PBS buffer (fig. 20, d), and after 5 min, PBS was replaced with the immobilization buffer (10 mM sodium acetate buffer, pH 4.8) for 2 min. (fig. 20, e). Then, GroES (1 mg/mL in the immobilization buffer) was added and left for 10 min. (fig. 20, f). Non-coupled ligand was removed by washing with PBS buffer for 2 min (fig. 20, g). Unreacted carboxylic groups, which could possibly interfere with the analysis were deactivated by a treatment with ethanolamine 1 M, pH 8.5 for 3 min (fig. 20, h), which also ensures the removal of any electrostatically bound material.

This step was followed by a wash with PBS, a wash with HCl 10 mM (regeneration buffer), and one last wash with PBS (fig. 20, i).

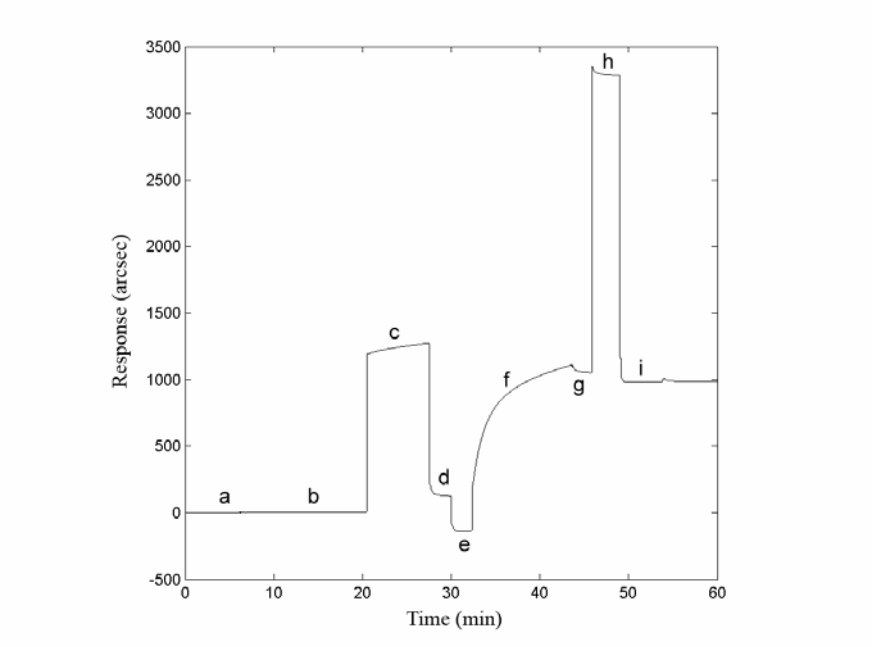


**Fig. 20:** Immobilization of GroEs of the carboxylate surface through NHS-EDC

The amount of immobilized ligand was calculated. Readout of about 900 arcseconds was obtained. These conditions resulted in the coupling of a "Langmuir" partial monolayer of a protein of 70 kDa. Then, both thymus and brain 20S proteasomes were added at increasing concentrations.

Regeneration steps were performed with PBS-T at pH 7.4 instead of more aggressive chemicals (HCl) because these latter could affect the stability of immobilized GroES and its functional ability to interact with soluble 20S proteasome. Binding data were analyzed with "Fast Fit software" (Fison Applied Sensor Technology), supplied with the instrument; this program uses

an iterative curve fitting to derive the observed rate constant and the maximum response at equilibrium due to ligand binding at a certain ligand concentration.

***Determination of the effects of GroES on the proteolytic activities of 20S proteasomes***

The effect of GroES on the proteolytic activities of the two proteasomes was evaluated through fluorescence assays. ChT-L, T-L, PGPH and BrAAP activity were determined using the peptides z-GGL-pNA, z-GGR-2NA, z-LLE-2NA, z-GPALG-pAB as substrates. The aminopeptidase N was used for the coupled assays in the determinations of the BrAAP activity.

Substrates for ChT-L, T-L and PGPH activities were dissolved in DMSO at a concentration of 10mM and then diluted till 0.5 mM with a Tris-HCl 50 mM pH 7.5 buffer. The substrate for the BrAAP activity was dissolved only in DMSO to a final concentration of 50mM. The mixture reaction was prepared for a final volume of 500 µl by adding in the following order:

- Tris-HCl buffer 50 mM pH 8
- 5 µg MPC
- Increasing amounts of GroES (1 mg/ml)
- Substrate

The reaction mixture was incubated at 37°C for 1 hour, and the fluorescence data were obtained on a Shimadzu RF-5301 PC fluorimeter by using appropriate wavelengths of emission and excitation, chosen in function of the fluorescent group bound to peptidic substrate.

Assays were conducted also in absence of GroES.

***Proteolytic Activity***

In order to assess the proteolytic activity of the 20S proteasome, β-casein was used: in fact, because of its partially unfolded structure, its hydrolysis by 20S proteasome mimes the *in vivo* degradation of proteins. The caseinolytic activity has been determined by incubating at 37°C 20µg of β-casein with 23 µg of 20S proteasome both in presence and absence of GroES in Tris(HCl) buffer 50mM, $MgCl_2$ pH 7.5 in a final volume of 20 µl. From the incubation mixture it has been pooled aliquots at sequential timing (2', 15', 30' and 60') and the reaction stopped by addition of 2µl of TCA 10%. The samples were then analyzed by HPLC with an RP column (Hamilton PRP3 equipped with pre-column). The elution has been made with a linear gradient till 90% with 0.1 % of TFA in 60 min at a flux of 1 ml/min. The degradation velocity has been evaluated by measuring the height of the chromatographic peak relative to the molecular substrate (λ= 210 nm) in function of time of incubation with the proteasome[104].

# RESULTS

## *Thermodynamics*

To understand the nature and the strength of the interaction between GroES from *E.Coli* and bovine proteasomes, binding studies using a resonant mirror biosensor were performed. The binding of soluble MPC to immobilized GroES was studied by adding a chosen concentration of bovine MPC in PBS and following the association kinetics up to equilibrium. The dissociation was obtained by addition of fresh PBS.

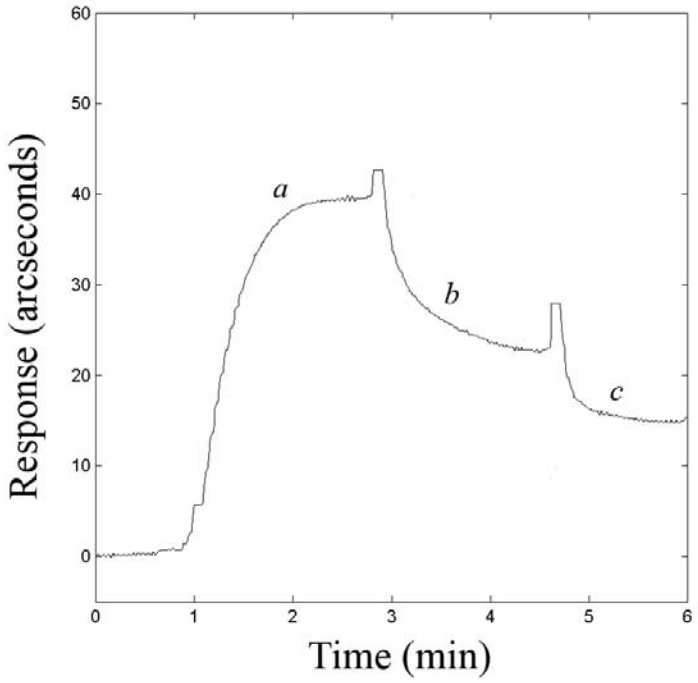


**Fig. 21:** Representative time course of 20S Proteasome binding to immobilized GroES: monophasic association (a) and dissociation (b) curve, and regeneration (c).

Then, MPCs were added at increasing concentration. At any titration step, baseline achievement was assessed before adding MPC, and then the regeneration steps were achieved as described in Experimental Procedures. In fig.22, monophasic association and dissociation time-courses of MPC both from thymus and brain binding to immobilized GroES are reported. These results were confirmed by F-Test performed on mono-exponential and bi-exponential models used to fit

experimental data: the probability of second phase being significant was not relevant for all the different time courses analysed (95% confidence).

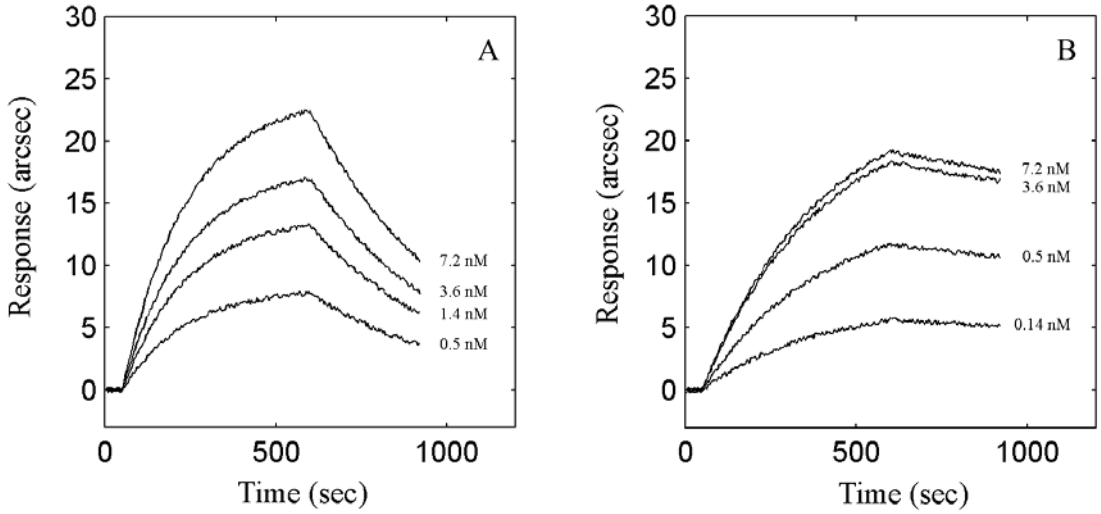


**Fig. 22:** MPC from brain (Box A) and thymus (Box B) binding to immobilized GroES: overlay of association and dissociation phases measured at increasing concentrations of MPC, pH=7.4.

The measured thermodynamic equilibrium constant for the $MPC_{brain}$ binding to GroES was ten folds higher with respect to $MPC_{thymus}$-GroES interaction ($K_{D,Brain}$ = [2.87±0.72] nM, $K_{D,Thymus}$ = [0.361±0.236] nM). The extent of binding (binding response at equilibrium) can be calculated for each time-course (at a given concentration of added GroES). The hyperbolic nature of the saturation plot in indicates non-cooperative binding of MPCs to GroES at pH 7.4.

***Kinetics***

Calculation of the association ($k_{ass}$) and dissociation ($k_{diss}$) rate constants for MPCs binding to GroES further defines the mechanistic properties of the macromolecular recognition process. The association phase allowed the measurement of the kinetic association constant, while the fast dissociation phase contributed to the high standard deviation associated to the dissociation constant (fig. 20, panel D). The standard deviations related to each kinetic association constant value $k_{ass}$ (each value was calculated from at least 5 association/dissociation kinetic experiments) are negligible because of the high precision experimental raw data (the instrument short-term noise is less than 1 arcsecond). Kinetic analysis of the binding of MPCs to GroES cleared the pathway of the two different recognition processes.

In fact, the analysis of kinetic constants revealed that the differences in equilibrium constants can be attributable exclusively to the slower dissociation step of GroES-$MPC_{Brain}$ complexes (kinetic

dissociation rate for $MPC_{Brain}$ was ten folds lower than $MPC_{Thymus}$), being the differences in the association process almost negligible within experimental error.

| | $k_{ass}$ ($M^{-1}s^{-1}$) | $k_{diss}$ ($ms^{-1}$) | $K_D$ (nM) |
|---|---|---|---|
| **$MPC_{Brain}$-GroES** | 748946±135521 | 0.27±0.17 | 0.361±0.236 |
| **$MPC_{Thymus}$-GroES** | 837613±113426 | 2.40±0.53 | 2.87±0.72 |

**Tab.5:** Equilibrium and kinetic constants for MPCs binding to immobilized GroES, pH 7.4

## *Fluorescence anisotropy*

Fluorescence polarization determinations were performed to obtain information on the possible interaction between quenched GroES and proteasomes from brain and thymus. This method is based on the photoselective excitation of fluorophore by polarized light. As a result of this selective excitation, a representative population of excited and oriented fluorophores randomly emits polarized light. The level of polarization, expressed as percentage anisotropy, is related to the fluorophore mobility: in fact, fluorophore mobility decreases at increasing anisotropy values. Dependences of percentage anisotropy for both proteasomes from molar ratio [MPC] / [GroES] are reported in fig.23. Percentage anisotropy gradually increases upon addition of soluble GroES to both MPCs: in particular, both proteasomes reached a plateau value approximately corresponding to a molar ratio [MPC]/[GroES] = 1, indicating a 1:1 stoichiometry.

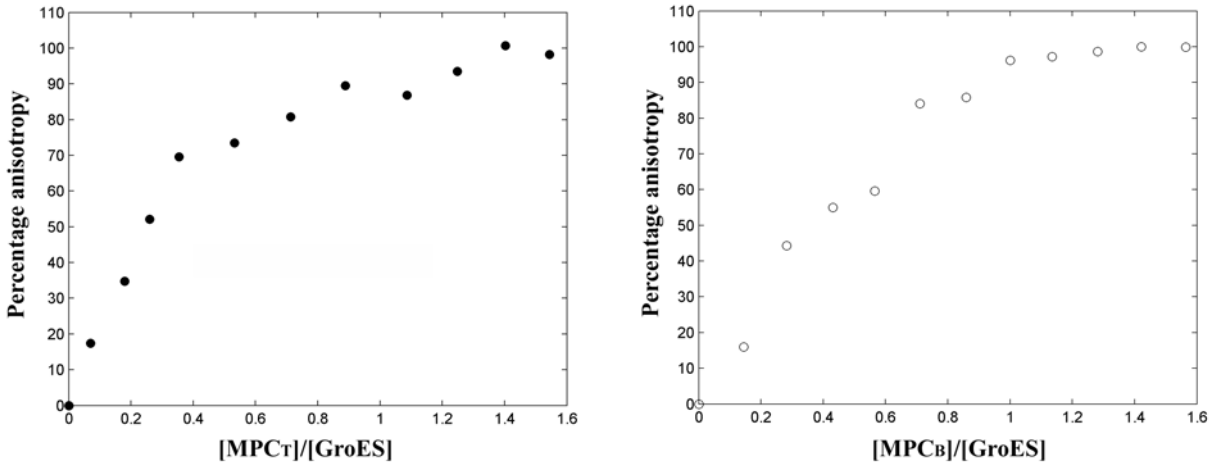


**Fig. 23:** Fluorescence polarization of Dansyl Chloride labeled GroES for MPCt (left box) and MPCb (right box); each value is the mean of six measurements (a mean 3% percentage standard error is associated to all experimental data; errorbars are omitted).

## *Role of GroES on the modulation of proteolytic activities of 20S proteasomes*

The effect exerted by GroES on proteolytic component of proteasomes purified both from bovine brain and thymus were tested in presence of increasing amount of GroES (from 0:1 to 1:1 GroES:Proteasome molar ratio). The dependence of percentage activity for ChT-L, BrAAP, T-L and PGPH from GroES:Proteasome molar ratio are reported, taking into account feasible interferences of sub-products (fig. 24).

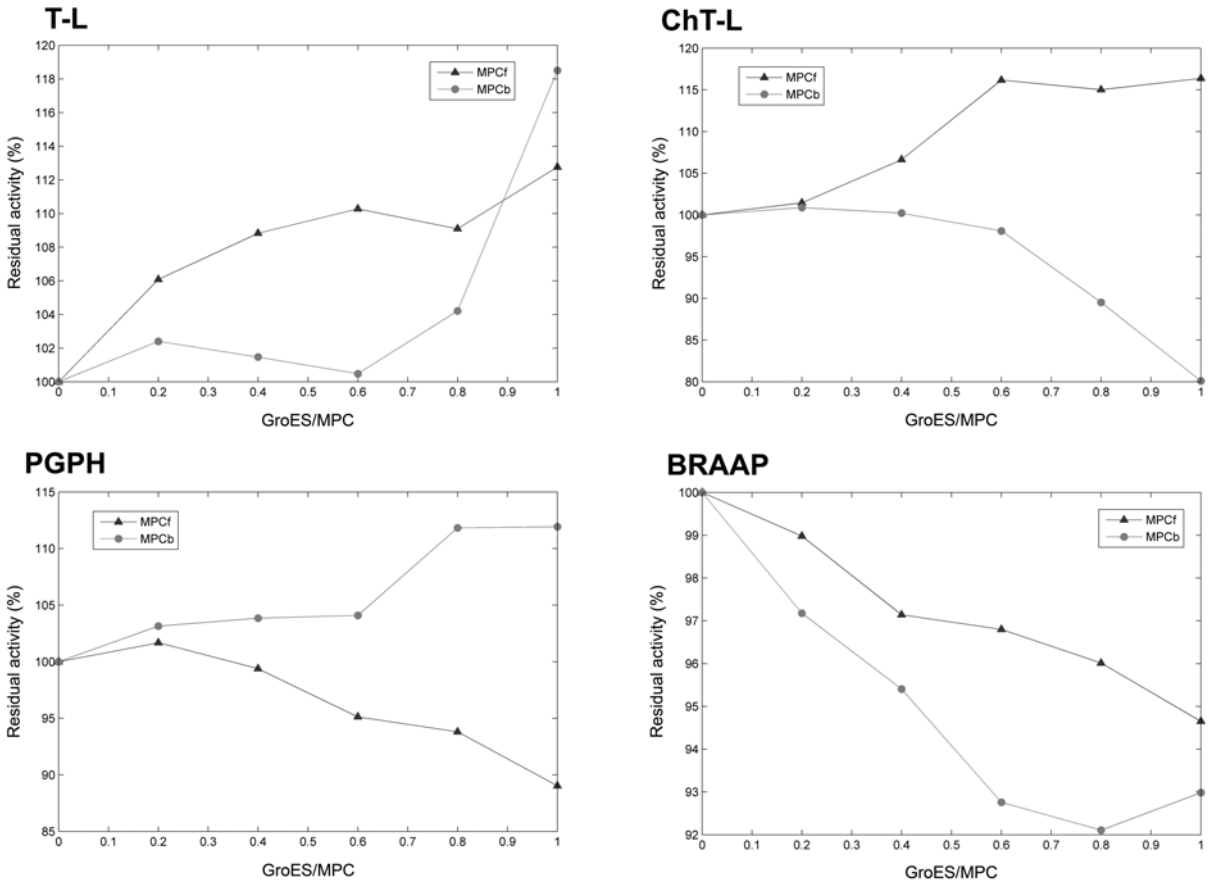


**Fig. 24:** Dependence of ChT-L, PGPH, T-L e BrAAP percentage residual activities from GroES:MPC molar ratio. Modualtion assays were performed as described in the experimental section. A mean 3% percentage standard error is associated to all experimental data; errorbars are omitted.

Obtained data revealed different effects induced by GroES on the two proteasomes.

In fact, ChT-L components from immuno and costitutive proteasomes were moderately activated and inhibited respectively, upon incubation with GroES (fig.24). An opposite behavior was reported for PGPH activity, weakly activated by GroES for constitutive proteasome, and inhibited for immuno proteasome. Differently, T-L activities were increased for both proteasomes, whereas BrAAP resulted mostly unaffected by GroES.

## *Effect of GroES on the degradation of β-casein*

Proteolytic activities of proteasomes were tested against β-casein, normally considered as pattern of partially unfolded proteins destined to degradation. Both proteasomes degraded β-casein, although immuno-proteasome showed higher rate of proteolysis.

The addition of GroES reduced caseinolytic activity of proteasome from brain, whilst no relevant effect was reported for proteasome from thymus (fig. 25).

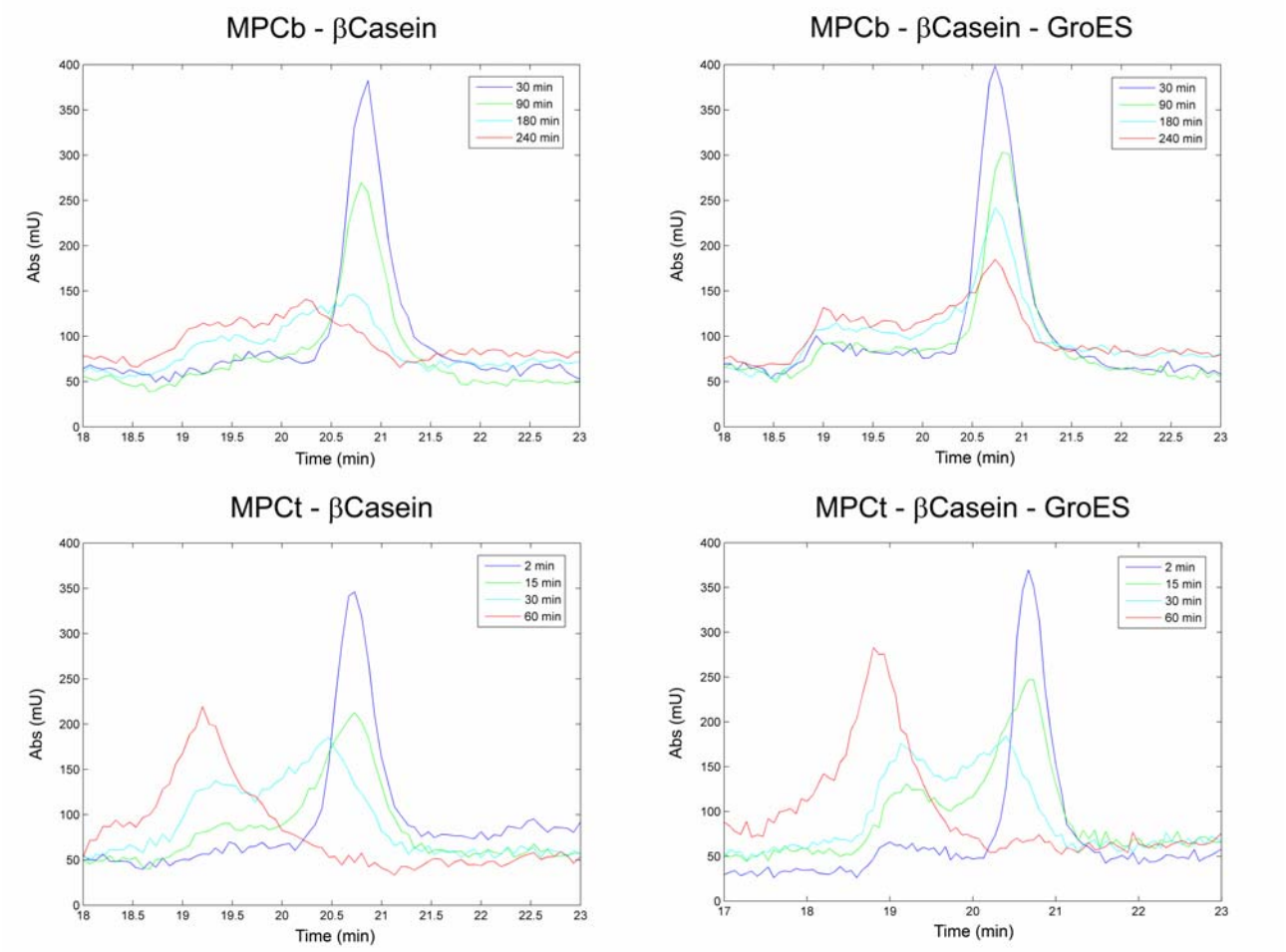


**Fig. 25:** Degradation of β-casein induced by Proteasomes in absence and in presence of GroES.

# CONCLUSION

The fast, simultaneous development of biopolymer databanks and proper analyzing software tools opened new scenarios in proteomics, representing a valuable *in silico* method for the prediction and the evaluation of possible interactions between two macromolecules. The bioinformatic approach discussed in Materials and Methods was here used to assess the interaction between the co-chaperonin GroES and MPC, this latter structurally resembling GroEL, GroES physiological partner. The identification of an established interaction between YML092c and YOR20c (two macromolecule belonging to MPC and GroES COGs, respectively) was the basis for the *in vitro* investigation of this interaction.

Anisotropy measurements reported two similar behaviors for MPC from brain and thymus upon titration with labeled GroES; in fact, according to this approach, both MPCs revealed the formation of a complex, characterized by a 1:1 stoichiometry (fig.23), consistently with earlier reported data for the GroES-GroEL complex[105]. In fact, since the affinity of the 1:1 GroEL-GroES complex for the second GroES oligomer was highly reduced due to the strong negative cooperativity between two binding sites, the 1:2 complex was highly unstable.

These considerations only refer to stable and high affinity complexes, not definitively precluding the possibility of transient 1:2 complexes formed upon the unfavorable addition of a second molecule of GroES. In this case, the 1:1 complex can be considered as an "acceptor state" for unfolded/damaged polypeptide destined to degradation.

SPR analysis allowed the determination of kinetics and thermodynamic parameters characterizing this interaction. Both proteasomes appeared to be able to bind GroES. In particular, equilibrium dissociation constants in nano- and subnano-molar range were reported for GroES binding to MPC from thymus and brain respectively. Collectively, kinetic and thermodynamic results ($k_{ass}$ in particular), suggested the presence of a high affinity binding-site for GroES on MPCs.

This characterization was highly interesting, since GroES showed an affinity fully comparable (even higher) in comparison with MPC physiological partner, Hsp90 [106].

Once confirmed the feasibility of this interaction, our interest was turned on the evaluation of a potential modulating effect on hydrolasic and proteolytic activities of MPCs by GroES. Mammalian 20S proteasome presents five hydrolasic activities, each differing in the residue involved in bond cleavage. These activities are associated to different β subunits, termed X, Y and Z, corresponding to ChT-L, PGPH, and T-L, whereas BrAAP and SNAAP are supposed to

depend upon a number of cooperating β subunits. Proteolytic activity is mainly related to ChT-L and BrAAP activities. The interaction between MPCs and GroES induced a moderate modulation on both activities. An increase in the T-L activity (for both MPCs) accompanied by a decrease in PGPH and ChT-L activities of MPC from brain was reported, while GroES enhanced PGPH and ChT-L activities of MPC from thymus. BrAAP activity of both MPCs was unaffected. Moreover, since the proteasome system is responsible for the degradation of various damaged proteins, we tested this the effect of GroES on the activity of 20S Proteasome toward β-casein, a macromolecule commonly considered as a pattern of partially unfolded proteins destined to degradation. Our experimental evidences revealed that the proteolytic activity of MPC from bovine brain was reduced upon incubation with GroES in a concentration dependent manner, whereas the activity of MPC from thymus was only weakly increased, being both behaviors in agreement with the above mentioned ChT-L modulation.

Additionally, GroES could affect the established proteasome ability to produce new oligo-peptides [107] by cleavage of precursor poly-peptide and catalysis of the formation of a new peptide bond between two distant fragments. This latter phenomenon is supposed to occur by transpeptidation as follows: cleavage by the proteasome is known to occur by nucleophilic attack of the peptide bond by the catalytic threonine, resulting in the formation of an acyl-enzyme intermediate in which a peptide fragment is attached by an ester bond to the catalytic threonine[108], producing an intermediate that comprises a target fragment attached to the catalytic threonine. Under normal condition, this intermediate would be readily hydrolyzed. Oppositely, within the confined catalytic chamber of the proteasome, the intermediate is surrounded by other peptide fragments, resulting from cleavage at other residues. The N-terminus of this fragment could compete with water molecules and occasionally make a nucleophilic attack of the ester bond of the intermediate, thereby forming a new peptide bond (fig.26).

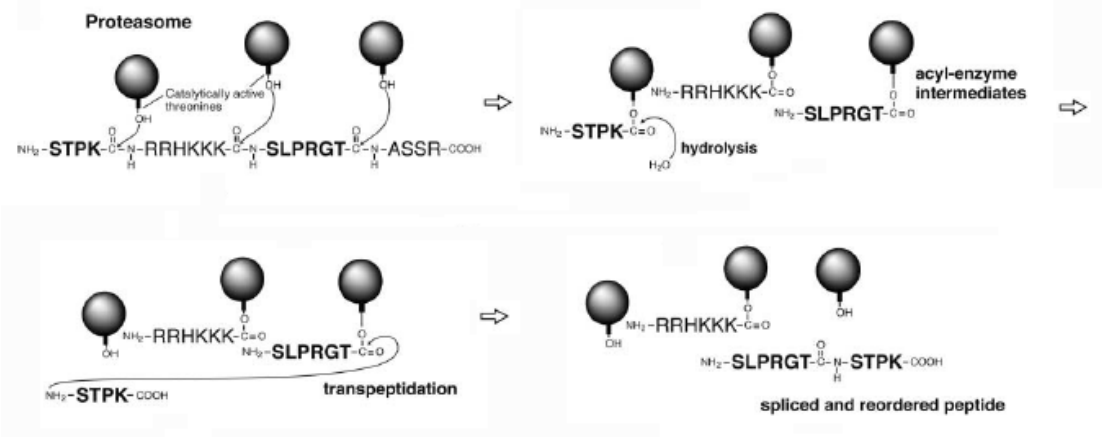


**Fig.26** Schematic representation of peptide splicing

The analysis of data obtained from proteolytic experiments and the template modeling of the GroES-MPC interface of binding based on GroES-GroEL crystal structure, suggested that the occlusion of the proteasomal cavity by GroES could enhance the protein splicing phenomenon, by reducing the number of water molecules (competing with N-fragment) available in the cavity.

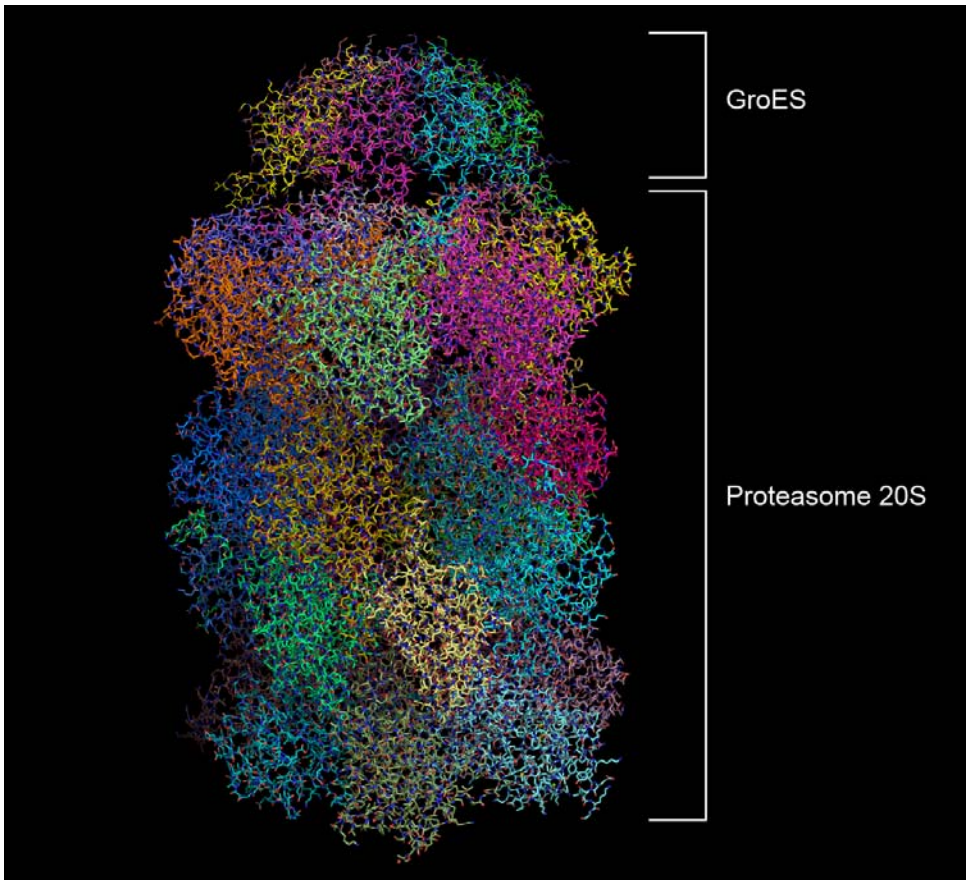


**Fig.27** MPC-GroES complex obtained from template modeling of GroEL-GroES crystal structure

Protein splicing has been described in unicellular organisms as the autocatalytic excision of segments termed inteins, which are up to several hundred amino acids in length[109]. It is catalyzed by the proteasome and therefore takes place during protein degradation. The ability of GroES to modulate proteasomal splicing of peptide fragments from a protein in either the initial or reverse order could have profound implications for the diversity of peptides that can be presented on the cell surface for recognition by systems directed to the detection and the elimination cells containing foreign or abnormal proteins.

Caseinolytic experiments revealed that GroES affects proteolysis rate but not the population peptide product (as judged from chromatographic profiles). However, the potential action of GroES as modulator of peptide splicing was not detected, possibly because of the low concentrated substrates (β-casein) used in these experiments: in fact, in the range of

concentration used, transpeptidation phenomena poorly compete with hydrolysis, since substrate products weakly displace water molecule.

In conclusion, the interaction between GroES and 20S proteasomes uncovers new scenarios on possible physio-pathological, related to the ability of proteasomes to interact both with unfolding- (Hsp90) and folding-assisting (GroES) proteins.

# REFERENCES


1. Bader GD, Betel D, Hogue CW. BIND: the Biomolecular Interaction Network Database. Nucleic Acids Res 2003;31(1):248-250.
2. Kanehisa M, Goto S, Kawashima S, Nakaya A. The KEGG databases at GenomeNet. Nucleic Acids Res 2002;30(1):42-46.
3. Xenarios I, Salwinski L, Duan XJ, Higney P, Kim SM, Eisenberg D. DIP, the Database of Interacting Proteins: a research tool for studying cellular networks of protein interactions. Nucleic Acids Res 2002;30(1):303-305.
4. Tatusov RL, Galperin MY, Natale DA, Koonin EV. The COG database: a tool for genome-scale analysis of protein functions and evolution. Nucleic Acids Res 2000;28(1):33-36.
5. Tatusov RL, Fedorova ND, Jackson JD, Jacobs AR, Kiryutin B, Koonin EV, Krylov DM, Mazumder R, Mekhedov SL, Nikolskaya AN, Rao BS, Smirnov S, Sverdlov AV, Vasudevan S, Wolf YI, Yin JJ, Natale DA. The COG database: an updated version includes eukaryotes. BMC Bioinformatics 2003;4:41.
6. Ito T, Chiba T, Yoshida M. Exploring the protein interactome using comprehensive two-hybrid projects. Trends Biotechnol 2001;19(10 Suppl):S23-27.
7. Ito T, Tashiro K, Muta S, Ozawa R, Chiba T, Nishizawa M, Yamamoto K, Kuhara S, Sakaki Y. Toward a protein-protein interaction map of the budding yeast: A comprehensive system to examine two-hybrid interactions in all possible combinations between the yeast proteins. Proc Natl Acad Sci U S A 2000;97(3):1143-1147.
8. Uetz P, Giot L, Cagney G, Mansfield TA, Judson RS, Knight JR, Lockshon D, Narayan V, Srinivasan M, Pochart P, Qureshi-Emili A, Li Y, Godwin B, Conover D, Kalbfleisch T, Vijayadamodar G, Yang M, Johnston M, Fields S, Rothberg JM. A comprehensive analysis of protein-protein interactions in Saccharomyces cerevisiae. Nature 2000;403(6770):623-627.
9. Gavin AC, Bosche M, Krause R, Grandi P, Marzioch M, Bauer A, Schultz J, Rick JM, Michon AM, Cruciat CM, Remor M, Hofert C, Schelder M, Brajenovic M, Ruffner H, Merino A, Klein K, Hudak M, Dickson D, Rudi T, Gnau V, Bauch A, Bastuck S, Huhse B, Leutwein C, Heurtier MA, Copley RR, Edelmann A, Querfurth E, Rybin V, Drewes G, Raida M, Bouwmeester T, Bork P, Seraphin B, Kuster B, Neubauer G, Superti-Furga G. Functional organization of the yeast proteome by systematic analysis of protein complexes. Nature 2002;415(6868):141-147.

10. Ho Y, Gruhler A, Heilbut A, Bader GD, Moore L, Adams SL, Millar A, Taylor P, Bennett K, Boutilier K, Yang L, Wolting C, Donaldson I, Schandorff S, Shewnarane J, Vo M, Taggart J, Goudreault M, Muskat B, Alfarano C, Dewar D, Lin Z, Michalickova K, Willems AR, Sassi H, Nielsen PA, Rasmussen KJ, Andersen JR, Johansen LE, Hansen LH, Jespersen H, Podtelejnikov A, Nielsen E, Crawford J, Poulsen V, Sorensen BD, Matthiesen J, Hendrickson RC, Gleeson F, Pawson T, Moran MF, Durocher D, Mann M, Hogue CW, Figeys D, Tyers M. Systematic identification of protein complexes in Saccharomyces cerevisiae by mass spectrometry. Nature 2002;415(6868):180-183.
11. Rain JC, Selig L, De Reuse H, Battaglia V, Reverdy C, Simon S, Lenzen G, Petel F, Wojcik J, Schachter V, Chemama Y, Labigne A, Legrain P. The protein-protein interaction map of Helicobacter pylori. Nature 2001;409(6817):211-215.
12. Humphreys K, Demetriou G, Gaizauskas R. Two applications of information extraction to biological science journal articles: enzyme interactions and protein structures. Pac Symp Biocomput 2000:505-516.
13. Proux D, Rechenmann F, Julliard L. A pragmatic information extraction strategy for gathering data on genetic interactions. Proc Int Conf Intell Syst Mol Biol 2000;8:279-285.
14. von Mering C, Krause R, Snel B, Cornell M, Oliver SG, Fields S, Bork P. Comparative assessment of large-scale data sets of protein-protein interactions. Nature 2002;417(6887):399-403.
15. Georgopoulos CP, Hendrix RW, Casjens SR, Kaiser AD. Host participation in bacteriophage lambda head assembly. J Mol Biol 1973;76(1):45-60.
16. Lorimer GH. A personal account of chaperonin history. Plant Physiol 2001;125(1):38-41.
17. Gething MJ, Sambrook J. Protein folding in the cell. Nature 1992;355(6355):33-45.
18. Zeilstra-Ryalls J, Fayet O, Georgopoulos C. The universally conserved GroE (Hsp60) chaperonins. Annu Rev Microbiol 1991;45:301-325.
19. Rospert S, Glick BS, Jeno P, Schatz G, Todd MJ, Lorimer GH, Viitanen PV. Identification and functional analysis of chaperonin 10, the groES homolog from yeast mitochondria. Proc Natl Acad Sci U S A 1993;90(23):10967-10971.
20. Viitanen PV, Lorimer GH, Seetharam R, Gupta RS, Oppenheim J, Thomas JO, Cowan NJ. Mammalian mitochondrial chaperonin 60 functions as a single toroidal ring. J Biol Chem 1992;267(2):695-698.

21. Bertsch U, Soll J, Seetharam R, Viitanen PV. Identification, characterization, and DNA sequence of a functional "double" groES-like chaperonin from chloroplasts of higher plants. Proc Natl Acad Sci U S A 1992;89(18):8696-8700.
22. Hendrix RW. Purification and properties of groE, a host protein involved in bacteriophage assembly. J Mol Biol 1979;129(3):375-392.
23. Saibil H, Dong Z, Wood S, auf der Mauer A. Binding of chaperonins. Nature 1991;353(6339):25-26.
24. Braig K, Simon M, Furuya F, Hainfeld JF, Horwich AL. A polypeptide bound by the chaperonin groEL is localized within a central cavity. Proc Natl Acad Sci U S A 1993;90(9):3978-3982.
25. Chen S, Roseman AM, Hunter AS, Wood SP, Burston SG, Ranson NA, Clarke AR, Saibil HR. Location of a folding protein and shape changes in GroEL-GroES complexes imaged by cryo-electron microscopy. Nature 1994;371(6494):261-264.
26. Langer T, Pfeifer G, Martin J, Baumeister W, Hartl FU. Chaperonin-mediated protein folding: GroES binds to one end of the GroEL cylinder, which accommodates the protein substrate within its central cavity. Embo J 1992;11(13):4757-4765.
27. Braig K, Otwinowski Z, Hegde R, Boisvert DC, Joachimiak A, Horwich AL, Sigler PB. The crystal structure of the bacterial chaperonin GroEL at 2.8 A. Nature 1994;371(6498):578-586.
28. Buckle AM, Zahn R, Fersht AR. A structural model for GroEL-polypeptide recognition. Proc Natl Acad Sci U S A 1997;94(8):3571-3575.
29. Chen L, Sigler PB. The crystal structure of a GroEL/peptide complex: plasticity as a basis for substrate diversity. Cell 1999;99(7):757-768.
30. Fenton WA, Kashi Y, Furtak K, Horwich AL. Residues in chaperonin GroEL required for polypeptide binding and release. Nature 1994;371(6498):614-619.
31. Xu Z, Horwich AL, Sigler PB. The crystal structure of the asymmetric GroEL-GroES-(ADP)7 chaperonin complex. Nature 1997;388(6644):741-750.
32. Hunt JF, Weaver AJ, Landry SJ, Gierasch L, Deisenhofer J. The crystal structure of the GroES co-chaperonin at 2.8 A resolution. Nature 1996;379(6560):37-45.
33. Landry SJ, Zeilstra-Ryalls J, Fayet O, Georgopoulos C, Gierasch LM. Characterization of a functionally important mobile domain of GroES. Nature 1993;364(6434):255-258.
34. Richardson A, Schwager F, Landry SJ, Georgopoulos C. The importance of a mobile loop in regulating chaperonin/ co-chaperonin interaction: humans versus Escherichia coli. J Biol Chem 2001;276(7):4981-4987.

35. Chandrasekhar GN, Tilly K, Woolford C, Hendrix R, Georgopoulos C. Purification and properties of the groES morphogenetic protein of Escherichia coli. J Biol Chem 1986;261(26):12414-12419.
36. Jackson GS, Staniforth RA, Halsall DJ, Atkinson T, Holbrook JJ, Clarke AR, Burston SG. Binding and hydrolysis of nucleotides in the chaperonin catalytic cycle: implications for the mechanism of assisted protein folding. Biochemistry 1993;32(10):2554-2563.
37. Roseman AM, Chen S, White H, Braig K, Saibil HR. The chaperonin ATPase cycle: mechanism of allosteric switching and movements of substrate-binding domains in GroEL. Cell 1996;87(2):241-251.
38. Azem A, Kessel M, Goloubinoff P. Characterization of a functional GroEL14(GroES7)2 chaperonin hetero-oligomer. Science 1994;265(5172):653-656.
39. Llorca O, Marco S, Carrascosa JL, Valpuesta JM. The formation of symmetrical GroEL-GroES complexes in the presence of ATP. FEBS Lett 1994;345(2-3):181-186.
40. Schmidt M, Rutkat K, Rachel R, Pfeifer G, Jaenicke R, Viitanen P, Lorimer G, Buchner J. Symmetric complexes of GroE chaperonins as part of the functional cycle. Science 1994;265(5172):656-659.
41. Weissman JS, Hohl CM, Kovalenko O, Kashi Y, Chen S, Braig K, Saibil HR, Fenton WA, Horwich AL. Mechanism of GroEL action: productive release of polypeptide from a sequestered position under GroES. Cell 1995;83(4):577-587.
42. Thirumalai D, Lorimer GH. Chaperonin-mediated protein folding. Annu Rev Biophys Biomol Struct 2001;30:245-269.
43. Weissman JS, Rye HS, Fenton WA, Beechem JM, Horwich AL. Characterization of the active intermediate of a GroEL-GroES-mediated protein folding reaction. Cell 1996;84(3):481-490.
44. Burston SG, Ranson NA, Clarke AR. The origins and consequences of asymmetry in the chaperonin reaction cycle. J Mol Biol 1995;249(1):138-152.
45. Gray TE, Fersht AR. Cooperativity in ATP hydrolysis by GroEL is increased by GroES. FEBS Lett 1991;292(1-2):254-258.
46. Yifrach O, Horovitz A. Two lines of allosteric communication in the oligomeric chaperonin GroEL are revealed by the single mutation Arg196-->Ala. J Mol Biol 1994;243(3):397-401.
47. Yifrach O, Horovitz A. Nested cooperativity in the ATPase activity of the oligomeric chaperonin GroEL. Biochemistry 1995;34(16):5303-5308.

48. Horovitz A, Fridmann Y, Kafri G, Yifrach O. Review: allostery in chaperonins. J Struct Biol 2001;135(2):104-114.
49. Rye HS, Roseman AM, Chen S, Furtak K, Fenton WA, Saibil HR, Horwich AL. GroEL-GroES cycling: ATP and nonnative polypeptide direct alternation of folding-active rings. Cell 1999;97(3):325-338.
50. Ranson NA, Burston SG, Clarke AR. Binding, encapsulation and ejection: substrate dynamics during a chaperonin-assisted folding reaction. J Mol Biol 1997;266(4):656-664.
51. Hayer-Hartl MK, Martin J, Hartl FU. Asymmetrical interaction of GroEL and GroES in the ATPase cycle of assisted protein folding. Science 1995;269(5225):836-841.
52. Rye HS, Burston SG, Fenton WA, Beechem JM, Xu Z, Sigler PB, Horwich AL. Distinct actions of cis and trans ATP within the double ring of the chaperonin GroEL. Nature 1997;388(6644):792-798.
53. Todd MJ, Viitanen PV, Lorimer GH. Dynamics of the chaperonin ATPase cycle: implications for facilitated protein folding. Science 1994;265(5172):659-666.
54. Mayhew M, da Silva AC, Martin J, Erdjument-Bromage H, Tempst P, Hartl FU. Protein folding in the central cavity of the GroEL-GroES chaperonin complex. Nature 1996;379(6564):420-426.
55. Chen J, Walter S, Horwich AL, Smith DL. Folding of malate dehydrogenase inside the GroEL-GroES cavity. Nat Struct Biol 2001;8(8):721-728.
56. Grallert H, Rutkat K, Buchner J. Limits of protein folding inside GroE complexes. J Biol Chem 2000;275(27):20424-20430.
57. Burston SG, Weissman JS, Farr GW, Fenton WA, Horwich AL. Release of both native and non-native proteins from a cis-only GroEL ternary complex. Nature 1996;383(6595):96-99.
58. Sparrer H, Rutkat K, Buchner J. Catalysis of protein folding by symmetric chaperone complexes. Proc Natl Acad Sci U S A 1997;94(4):1096-1100.
59. Ewalt KL, Hendrick JP, Houry WA, Hartl FU. In vivo observation of polypeptide flux through the bacterial chaperonin system. Cell 1997;90(3):491-500.
60. Sakikawa C, Taguchi H, Makino Y, Yoshida M. On the maximum size of proteins to stay and fold in the cavity of GroEL underneath GroES. J Biol Chem 1999;274(30):21251-21256.
61. Baumeister W, Walz J, Zuhl F, Seemuller E. The proteasome: paradigm of a self-compartmentalizing protease. Cell 1998;92(3):367-380.

62. Bochtler M, Ditzel L, Groll M, Hartmann C, Huber R. The proteasome. Annu Rev Biophys Biomol Struct 1999;28:295-317.
63. DeMartino GN, Slaughter CA. The proteasome, a novel protease regulated by multiple mechanisms. J Biol Chem 1999;274(32):22123-22126.
64. Groll M, Ditzel L, Lowe J, Stock D, Bochtler M, Bartunik HD, Huber R. Structure of 20S proteasome from yeast at 2.4 A resolution. Nature 1997;386(6624):463-471.
65. Lowe J, Stock D, Jap B, Zwickl P, Baumeister W, Huber R. Crystal structure of the 20S proteasome from the archaeon T. acidophilum at 3.4 A resolution. Science 1995;268(5210):533-539.
66. Dick TP, Nussbaum AK, Deeg M, Heinemeyer W, Groll M, Schirle M, Keilholz W, Stevanovic S, Wolf DH, Huber R, Rammensee HG, Schild H. Contribution of proteasomal beta-subunits to the cleavage of peptide substrates analyzed with yeast mutants. J Biol Chem 1998;273(40):25637-25646.
67. Orlowski M, Wilk S. Catalytic activities of the 20 S proteasome, a multicatalytic proteinase complex. Arch Biochem Biophys 2000;383(1):1-16.
68. Coux O, Tanaka K, Goldberg AL. Structure and functions of the 20S and 26S proteasomes. Annu Rev Biochem 1996;65:801-847.
69. Lehner PJ, Cresswell P. Processing and delivery of peptides presented by MHC class I molecules. Curr Opin Immunol 1996;8(1):59-67.
70. Ortiz-Navarrete V, Seelig A, Gernold M, Frentzel S, Kloetzel PM, Hammerling GJ. Subunit of the '20S' proteasome (multicatalytic proteinase) encoded by the major histocompatibility complex. Nature 1991;353(6345):662-664.
71. Tanaka K. Role of proteasomes modified by interferon-gamma in antigen processing. J Leukoc Biol 1994;56(5):571-575.
72. Almenoff J, Orlowski M. Membrane-bound kidney neutral metalloendopeptidase: interaction with synthetic substrates, natural peptides, and inhibitors. Biochemistry 1983;22(3):590-599.
73. Eleuteri AM, Angeletti M, Lupidi G, Tacconi R, Bini L, Fioretti E. Isolation and characterization of bovine thymus multicatalytic proteinase complex. Protein Expr Purif 2000;18(2):160-168.
74. Lowry OH, Rosebrough NJ, Farr AL, Randall RJ. Protein measurement with the Folin phenol reagent. J Biol Chem 1951;193(1):265-275.
75. Bradford MM. A rapid and sensitive method for the quantitation of microgram quantities of protein utilizing the principle of protein-dye binding. Anal Biochem 1976;72:248-254.

76. Wood RW. On a remarkable case of uneven distribution of light in a diffraction grating spectrum. Phil Magm 1902(4):396–402.
77. Kretschmann E, Raether, H. Radiative decay of non-radiative surface plasmons excited by light. Z Naturforsch 1968(23A):2135–2136.
78. Otto A. Excitation of surface plasma waves in silver by the method of frustrated total reflection. Z Physik 1968(216):398–410.
79. Raether H. Surface plasmons on smooth and rough surfaces and on gratings. Berlin; 1988.
80. Nylander C, Liedberg, B., Lind, T. Gas detection by means of surface plasmons resonance. Sensors and Actuators 1982(3):79-88.
81. Matsubara K, Kawata, S., Minami, S. Optical chemical sensor based on surface plasmon measurement. Appl Opt 1988(27):1160–1163.
82. Zhang LM, Uttamchandani, D. Optical chemical sensing employing surface plasmon resonance. Electron Lett 1988(23):1469–1470.
83. Homola J. On the sensitivity of surface plasmon resonance sensors with spectral interrogation. Sensors and Actuators B 1997(41):207-211.
84. de Bruijn HE, Altenburg, B.S.F., Kooyman, R.P.H., Greve, J. Choice of metal and wavelength for surface-plasmon resonance sensors: some considerations. Appl Opt 1992(31):440–442.
85. Herminghaus SL, P. Improved attenuated total reflectance technique for the investigation of dielectric surfaces. Appl Phys Lett 1989(54):99–101.
86. Podgorsek RP, Sandten, U., Franke, H., Woods, J. Monitoring of diffusion of vapor molecules in polymer films using SPRleaky- mode spectroscopy. 1997; Munster, Germany. p 247–248.
87. Phelps JM, Taylor, D.M. Determining the relative permittivity and thickness of a lossless dielectric overlayer on a metal film using optically excited surface plasmon polaritons. J Phys D (Applied Physics) 1996(29):1080–1087.
88. Boardman AD. Electromagnetic surface modes. Wiley, editor. Chichester; 1982.
89. Homola J, Yee, S., Myszka, D. Surface plasmon biosensors. Ligler FS TCe, editor: Elsevier; 2002.
90. Snyder AW, Love, J.D. Optical waveguide theory. London: Chapman and Hall; 1983.
91. Reather H. Surface plasmons on smooth and rough surfaces and on gratings, Springer tracts in modern physics. New York; 1983.
92. Hutley MC. Diffration gratings: Academic Press, London; 1982.

93. Edwards PR, Leatherbarrow RJ. Determination of association rate constants by an optical biosensor using initial rate analysis. Anal Biochem 1997;246(1):1-6.
94. Welfle K, Misselwitz R, Hausdorf G, Hohne W, Welfle H. Conformation, pH-induced conformational changes, and thermal unfolding of anti-p24 (HIV-1) monoclonal antibody CB4-1 and its Fab and Fc fragments. Biochim Biophys Acta 1999;1431(1):120-131.
95. Berlman IB. Handbook of fuorescence Spectra of aromatic molecules. Academic Press, New York, Second Edition 1971.
96. Kasha M. Disc Faraday Soc 1950;9(14).
97. Stokes GG. Phil Trans R Soc London 1852;142(463).
98. Waggoner A. Covalent labeling of proteins and nucleic acids with fluorophores. Methods Enzymol 1995;246:362-373.
99. Azumi T, McGlynn SP. J Chem Phys 1962;37: 2413.
100. Lakowicz JR. Principles of Fluorescence Spectroscopy. Plenum, New York 1983.
101. Laemmli UK. Cleavage of structural proteins during the assembly of the head of bacteriophage T4. Nature 1970;227(5259):680-685.
102. Seale JW, Gorovits BM, Ybarra J, Horowitz PM. Reversible oligomerization and denaturation of the chaperonin GroES. Biochemistry 1996;35(13):4079-4083.
103. Edwards PR, Lowe PA, Leatherbarrow RJ. Ligand loading at the surface of an optical biosensor and its effect upon the kinetics of protein-protein interactions. J Mol Recognit 1997;10(3):128-134.
104. Eleuteri AM, Kohanski RA, Cardozo C, Orlowski. M J Biol Chem 1997;272:11824-11183.
105. Gorovits BM, Ybarra J, Seale JW, Horowitz PM. Conditions for nucleotide-dependent GroES-GroEL interactions. GroEL14(groES7)2 is favored by an asymmetric distribution of nucleotides. J Biol Chem 1997;272(43):26999-27004.
106. Eleuteri AM, Cuccioloni M, Bellesi J, Lupidi G, Fioretti E, Angeletti M. Interaction of Hsp90 with 20S proteasome: thermodynamic and kinetic characterization. Proteins 2002;48(2):169-177.
107. Vigneron N, Stroobant V, Chapiro J, Ooms A, Degiovanni G, Morel S, van der Bruggen P, Boon T, Van den Eynde BJ. An antigenic peptide produced by peptide splicing in the proteasome. Science 2004;304(5670):587-590.
108. Groll M, Huber R. Substrate access and processing by the 20S proteasome core particle. Int J Biochem Cell Biol 2003;35(5):606-616.

109. Paulus H. Protein splicing and related forms of protein autoprocessing. Annu Rev Biochem 2000;69:447-496.